Structural insights into perilipin 3 membrane association in response to diacylglycerol accumulation

Yong Mi Choi[1a], Dalila Ajjaji[2a], Kaelin D. Fleming[3], Peter P. Borbat[4,5], Meredith L. Jenkins[3], Brandon E. Moeller[3], Shaveen Fernando[6], Surita R. Bhatia[6], Jack H. Freed[4,5], John E. Burke[3,7*], Abdou Rachid Thiam[2*], Michael V. Airola[1*]

[1]Department of Biochemistry and Cell Biology, Stony Brook University, Stony Brook NY 11794, USA
[2]Laboratoire de Physique de l'École normale supérieure, ENS, Université PSL, CNRS, Sorbonne Université, Université Paris Cité, F-75005 Paris, France
[3]Department of Biochemistry and Microbiology, University of Victoria, Victoria BC V8N 1A1, Canada
[4]National Biomedical Resource for Advanced Electron Spin Resonance Technology (ACERT), Cornell University, Ithaca NY 14853, USA
[5]Department of Chemistry and Chemical Biology, Cornell University, Ithaca NY 14853, USA
[6]Department of Chemistry, Stony Brook University, Stony Brook NY 11794, USA
[7]Department of Biochemistry and Molecular Biology, The University of British Columbia, Vancouver, British Columbia V6T 1Z3, Canada

[a]These authors contributed equally

*Address correspondence to:
Michael V. Airola, michael.airola@stonybrook.edu
Abdou Rachid Thiam, thiam@ens.fr
John E. Burke, jeburke@uvic.ca

ABSTRACT

Lipid droplets (LDs) are dynamic organelles that contain an oil core mainly composed of triglycerides (TAG) that is surrounded by a phospholipid monolayer and LD-associated proteins called perilipins (PLINs). During LD biogenesis, perilipin 3 (PLIN3) is recruited to nascent LDs as they emerge from the endoplasmic reticulum. Here, we analyzed how lipid composition affects PLIN3 recruitment to membrane bilayers and LDs, and the structural changes that occur upon membrane binding. We found the TAG precursors phosphatidic acid and diacylglycerol (DAG) recruit PLIN3 to membrane bilayers and define an expanded Perilipin-ADRP-Tip47 (PAT) domain that preferentially binds DAG enriched membranes. Membrane binding induces a disorder/order transition of alpha helices within the PAT domain and 11-mer repeats, with intramolecular distance measurements consistent with the expanded PAT domain adopting a folded but dynamic structure upon membrane binding. In cells, PLIN3 is recruited to DAG enriched ER membranes, and this requires both the PAT domain and 11-mer repeats. This provides molecular details of PLIN3 recruitment to nascent LDs and identifies a function of the PAT domain of PLIN3 in DAG binding.

INTRODUCTION

Lipid droplets (LDs) act as energy reservoirs in cells. They contain a neutral lipid core of mainly triacylglycerols (TAGs) and cholesterol esters with a phospholipid monolayer that surrounds the neutral lipid core. This creates a membrane environment for LDs that is distinct from membrane bilayers and recruits several LD-associated proteins [1-3]. In addition to a major role in energy storage, LDs are also important cellular hubs that traffic proteins and lipids between organelles, regulate ER stress, and contribute to viral infections [4-6].

LDs are formed in the ER where neutral lipids are synthesized [7, 8]. Mechanistically, LD formation involves several steps [9] including accumulation of neutral lipids in the outer ER membrane leaflet, neutral lipid nucleation aided by the seipin complex and associated factors (e.g. LDAF1) [10], formation of nascent LDs that bud from the ER [11, 12] and LD growth and maturation [13, 14]. Several lines of evidence support the idea that the phospholipid composition of the ER membrane is locally edited to promote LD assembly or recruit specific proteins important for LD formation such as seipin and ORP proteins [7, 15-17]. Although there is still uncertainty regarding the phospholipid composition at the initial stages of LD formation, evidence from yeast suggest diacylglycerol (DAG), the direct precursor of TAG, is enriched in discrete ER subdomains where LD biogenesis is initiated [15, 18]. DAG can also promote TAG nucleation and impact the architecture of LDs on the ER [15, 19].

Perilipins (PLINs) are the major class of proteins that coat the surface of LDs [20-26]. There are five PLINs in humans that bind LDs at various stages of their initiation and maturation [21]. For example, PLIN1 is the major PLIN that binds to mature LDs in adipocytes, while PLIN2 and PLIN5 reside on mature LDs in liver and muscle cells, respectively [27]. In contrast, PLIN3 displays near ubiquitous expression and binds to early LDs as they bud from the ER but is later displaced by other PLINs as LDs grow and mature [10, 28]. PLIN3 is stable and not degraded in the absence of LDs. This allows PLIN3 to translocate from the cytoplasm to sites of early LD formation, where PLIN3 is well established to act as a marker for the biogenesis of early LDs across species [10, 28, 29].

PLINs share a conserved protein domain architecture composed of an N-terminal PAT domain, followed by variable stretches of 11-mer repeats and a C-terminal 4-helix bundle [30, 31]. The 11-mer repeats form amphipathic helixes that are sufficient to recruit PLINs to LDs [30-32], while the

83 4-helix bundle in some PLINs can also bind LDs [30, 33]. The binding of amphipathic helices,
84 such as those found in the 11-mer repeats, to membrane interfaces is greatly influenced by the
85 level or presence of phospholipid packing defects [34, 35]. The degree of packing is determined
86 by the type of lipid present (as indicated in the triangle in **Fig. 1A**). When it comes to the oil-water
87 interface of LDs, the recruitment of amphipathic helices is greater when the level of phospholipid
88 packing is lower [35, 36], i.e. when there are more packing defects. Although the PAT domain is
89 the most conserved domain among PLINs, its function is not clear, as it has not been
90 demonstrated to bind to membranes or LDs.
91
92 Here, we examine the mechanism of PLIN3 recruitment to membrane bilayers and LDs using a
93 combination of *in vitro* and cell culture assays, and analyze the structural changes induced by
94 membrane binding using hydrogen-deuterium exchange mass spectrometry (HDX-MS) and
95 pulsed-dipolar electron spin resonance spectroscopy (PD-ESR). We found that human PLIN3 is
96 recruited to membrane bilayers enriched in the TAG precursors phosphatidic acid (PA) and DAG.
97 By delineating the roles of the PAT domain and 11-mer repeats, we define an expanded PAT
98 domain that is sufficient for PLIN3 to bind DAG enriched membranes, while the 11-mer repeats
99 are sufficient to bind LD monolayers. We confirm that DAG enrichment can drive PLIN3
100 recruitment to ER membranes in cells, and this requires both the PAT domain and 11-mer repeats.
101 Structurally, the PAT domain and 11-mer repeats form inducible alpha helices to drive membrane
102 association and the PAT domain forms a tertiary structure upon membrane binding. Taken
103 together, this study provides molecular insight into how PLIN3 is recruited to early LDs and reveals
104 a novel function for the PAT domain of PLIN3 in DAG binding.
105
106
107

RESULTS

The Triglyceride Precursors DAG and PA Recruit PLIN3 to Membrane Bilayers

To systematically define how lipid composition affects PLIN3 recruitment to membrane bilayers, we purified recombinant human PLIN3 from *Escherichia coli* and used liposome co-sedimentation assays to monitor membrane binding. Liposomes were prepared using multiple freeze/thaw cycles and characterized by dynamic light scattering (DLS) **(Fig. S1A)**. Liposomes were made from phospholipids with different acyl-chain combinations comprised of either palmitoyl-oleoyl (PO) or di-oleoyl (DO) phospholipids **(Fig. 1A)**. PO phospholipids have one unsaturated acyl chain and are representative of the typical lipid composition in ER membranes. DO phospholipids contain two unsaturated acyl chains, have increased membrane packing defects [34, 37-39] and are enriched in ER membranes after oleate supplementation, which stimulates LD formation [15, 40-42]. Initial liposome co-sedimentation experiments varied the ratio of neutral phospholipids phosphatidylcholine (PC) and phosphatidylethanolamine (PE), as PC and PE represent the major lipids on both the cytoplasmic face of the ER and surface of LDs, PE increases both PLIN2 binding to liposomes [43] and PLIN3 insertion into mixed lipid monolayers at phospholipid-oil interfaces [44] and the ratio of PC to PE has previously been shown to regulate protein distribution on LDs [43, 45]. Under all PC-to-PE ratios tested, PLIN3 did not bind liposomes comprised solely of PC and PE **(Fig. 1B)**.

We next asked whether addition of other lipids that are synthesized in the ER could recruit PLIN3 to membranes by generating PC/PE liposomes containing 20mol% of either phosphatidic acid (PA), phosphatidylserine (PS), diacylglycerol (DAG), phosphatidylinositol (PI) or C18:1 ceramide. Regardless of lipid composition, PLIN3 did not bind to any PO-based liposomes **(Fig. 1C, 1D)**. However, PLIN3 was recruited to DO-based liposomes enriched in DAG or PA [37, 38, 46] **(Fig. 1C, 1D)**. Addition of DOPS and ceramide resulted in a minor increase in PLIN3 binding in DO-based liposomes, while the addition of PI had no effect **(Fig. 1C, 1D)**.

PLIN3 recruitment to DO-based liposomes depended on the surface concentration of DAG, with 5mol% DAG able to induce ~10% binding, and 20mol% DAG inducing 35% binding **(Fig. 1E)**. The addition of DOPA further increased PLIN3 binding in DAG-containing liposomes, which suggested a synergistic effect of PA and DAG on PLIN3 membrane recruitment **(Fig. 1F)**. Increasing the total liposome concentration caused the majority of PLIN3 to bind membranes, but 5% of PLIN3 remained in the soluble fraction **(Fig. S2A)**. DLS characterization indicated DAG enriched

141 liposomes had two populations based on size **(Fig. S1C, S1D)**, which is likely due to the fusogenic
142 properties of DAG [46]. The addition of DOPA or PLIN3 protein decreased or eliminated the
143 population of the larger (>400 nm) liposomes **(Fig. S1C, S1D)**. We concluded that PLIN3 binds
144 liposomes containing DAG and/or PA, which are notably the membrane-lipid precursors for
145 triglyceride synthesis, and PLIN3 can also remodel membranes, consistent with previous studies
146 [29].
147
148 **PLIN3 Binds to Liposomes with Membrane Packing Defects**
149 LDs have increased membrane packing defects in comparison to membrane bilayers [47].
150 Previously, PLIN4 has been shown to have increased binding to liposomes composed of methyl
151 branched diphytanoyl (4ME) phospholipids that create shallow lipid-packing defects that can be
152 accessed by hydrophobic insertion of peripheral membrane proteins, such as PLINs [31, 48]. The
153 packing defects induced by 4ME phospholipids are greater than DO phospholipids because of
154 the wider space between lipids [48]. In comparison to DO and PO liposomes, 4ME phospholipids
155 significantly increased PLIN3 liposome association with ~70% binding observed with a mixture of
156 4ME-PC and 4ME-PE **(Fig. 1G)**. Consistent with our previous observations, 4ME-PA further
157 increased PLIN3 binding, while 4ME-PS and C18:1 ceramide decreased binding **(Fig. 1G)**. The
158 effect of DAG was unable to be assessed as addition of DAG to 4ME-PC/PE disrupted proper
159 liposome formation. Taken together, this suggests PLIN3 membrane binding is also dependent
160 on lipid packing defects, and PA can further enhance PLIN3 membrane binding.
161
162 **PLIN3 Binding to Artificial Lipid Droplets**
163 As the major function of PLIN3 is to bind to emerging LDs as they bud from the ER, we next
164 assessed the ability of recombinant PLIN3 to bind artificial lipid droplets (ALDs) *in vitro* using a
165 flotation assay [10, 28, 29, 49]. ALDs were generated with a triolein neutral lipid core surrounded
166 by a phospholipid monolayer of DOPC and DOPE in 1:2.5 molar ratio of phospholipids to TAG.
167 ALDs with 80mol% DOPC and 20mol% DOPE showed 50% binding of PLIN3 **(Fig. S2B)**. The
168 addition of the anionic phospholipids PI4P decreased PLIN3 binding to ALDs. In contrast, PA, PS
169 and PI slightly decreased binding, ceramide did not affect binding, and DAG slightly increased
170 PLIN3 binding. However, none of these effects were statistically significant. The modest impact
171 of these PA, PS, PI, DAG, and ceramide, which all can induce negative curvature or charge in
172 membrane bilayers, may be due to the basal occurrence of significant phospholipid packing voids

173 on the ALD surface as compared with bilayers [36, 47]; while the strongly charged PI4P would
174 instead mask these and diminish binding [47].
175
176 **The PAT Domain and 11-mer Repeats are Disordered in the Absence of Membranes**
177 We next sought to examine how the structure of PLIN3 changes upon membrane binding, first
178 focusing on the structure of PLIN3 in the absence of membranes. For these experiments, we used
179 hydrogen deuterium exchange mass spectrometry (HDX-MS), which measures the exchange of
180 amide hydrogens with deuterated solvent. This method acts as a readout for protein
181 conformational dynamics with regions that form secondary structures undergoing slower
182 deuterium exchange than disordered regions, which lack intramolecular hydrogen bonds and
183 secondary structure [50, 51]. A brief pulse of deuterated solvent is useful for identifying regions
184 within a protein that lack structure compared to ordered regions [52, 53].
185
186 We determined the absolute exchange of PLIN3 after a 3sec pulse of deuterium incorporation at
187 0°C (equivalent to ~0.3sec at 20°C) using a fully deuterated control. After the deuterium pulse,
188 the first 200 residues of PLIN3 comprising the PAT domain and 11-mer repeats were fully
189 deuterated, indicating these regions are completely disordered in the absence of membranes **(Fig.**
190 **2A)**. The 4-helix bundle and α/β domain were largely ordered with comparatively low rates of
191 deuterium incorporation **(Fig. 2A)**, which is consistent with prior structural studies of PLIN3 [54,
192 55].
193
194 **The PAT Domain and 11-mer Repeats are the Major Drivers of PLIN3 Membrane**
195 **Association**
196 We next sought to determine any conformational changes that occur during membrane binding
197 using HDX-MS. Having established optimal conditions for PLIN3 membrane binding, we
198 measured the deuterium exchange rate over various time points (3, 30, 300, and 3000sec) in the
199 absence or presence of 4ME liposomes composed of 60mol% 4ME-PC, 20mol% 4ME-PE, and
200 20mol% 4ME-PA.
201
202 In the presence of membranes, striking differences in deuterium exchange were observed
203 throughout the PLIN3 sequence **(Fig. 2E, Table S1, source data)**. The most notable differences
204 were large decreases in deuterium exchange in the PAT domain and 11-mer repeat regions. In

205 comparison to previous results that demonstrated the 11-mer repeats are sufficient for the lipid
206 droplet association [30, 31], this suggests that the PAT domain and 11-mer repeats are both major
207 contributors to membrane binding. Consistently, we found that a purified PAT/11-mer repeats
208 fragment displayed similar membrane recruitment as full length PLIN3 to DO liposomes enriched
209 in DAG and PA, and 4ME liposomes **(Fig. 2C, 2D)**.
210
211 The HDX-MS results suggested that membrane binding induces the formation of a secondary
212 structure in the PAT domain and 11-mer repeats. This is consistent with both AlphaFold and
213 RoseTTAFold models that predict the PAT domain and 11-mer repeats form amphipathic alpha
214 helices, with the PAT domain adopting a triangular globular structure and the 11-mer repeats
215 forming a series of extended alpha helices **(Fig. 2B, 3B)**. Based on these results we concluded
216 that the PAT domain and 11-mer repeats of PLIN3 are intrinsically disordered in the absence of
217 membranes, with inducible amphipathic alpha helices being stabilized upon membrane binding.
218
219 Notably, many of the peptides with the PAT domain and 11-mer repeats displayed a bimodal
220 distribution of deuterium exchange upon membrane binding **(Fig. S3A, S3B)**. This differs from a
221 canonical distribution where the degree of deuteriation is gaussian in individual peptides. The
222 observed bimodal distributions are consistent with either EX1 exchange [56], or there being two
223 distinct protein conformations in the sample. Depending on the membrane residency of PLIN3,
224 bimodal distributions can be consistent with observations of the free and membrane bound state.
225 Given our previous observation that the PAT and 11-mer repeats are intrinsically disordered in
226 the absence of membranes, the simplest interpretation is that the PAT domain and 11-mer
227 repeats cycle between two states: 1) a membrane bound alpha helical state on membranes that
228 is strongly protected from H-D exchange and 2) an intrinsically disordered solution state that
229 rapidly exchanges with deuterated solvent upon dissociation from membranes and leads to rapid
230 H-D exchange. Therefore, the half-life of bimodal exchange can act as a surrogate for membrane
231 residency time for disordered regions of the protein.
232
233 The protection from deuterium exchange and the non-gaussian bimodal distribution for most
234 peptides in the PAT domain persisted over a longer time course (~300sec) in comparison to
235 peptides within the 11-mer repeat regions (~30sec) **(Fig. S4A)**. This trend of longer HDX
236 protection correlated with the degree of sequence conservation among PLINs **(Fig. 3A)**. Taken

237 together this supports a role for the PAT domain in membrane binding and suggests a similar role
238 for the highly conserved PAT domain in other PLINs.
239
240 In contrast to the N-terminal PAT domain and 11-mer repeats, the C-terminal 4-helix bundle
241 displayed a large increase in deuterium exchange **(Fig. 2E, S4A)**. The most apparent increase in
242 deuterium exchange was in the middle of the 4-helix bundle. We hypothesized this was due to
243 the 4-helix bundle unfolding upon membrane binding, with this possibly contributing to membrane
244 recruitment. To test this, we examined the ability of a purified PLIN3 4-helix bundle fragment
245 (residues 197-427) to bind membranes. Consistent with our hypotheses, the isolated 4-helix
246 bundle bound to the 4ME-PC/PE/PA liposomes that were used in the HDX-MS experiment **(Fig.**
247 **2C, 2D)**. However, the 4-helix bundle did not bind to 4ME-liposomes lacking PA, or to any DO-
248 based liposomes even when PA and DAG were present **(Fig. 2C, 2D)**. We concluded that the 4-
249 helix bundle of PLIN3 can unfold and bind membranes, but only under very specific condition
250 such as the presence of accumulated PA on the membrane having packing defects induced by
251 4ME-PC/PE. This conclusion is supported by the PA accumulation at the nascent LD formation
252 stie where lipid packing defects occur [17].
253
254 To understand how lipid composition influences the structure of PLIN3, we again applied HDX-
255 MS, using variable liposome compositions of 4ME-PC/PE and DOPC/PE/DAG **(Fig. 2F, 2G)**. In
256 line with of previous HDX-MS and liposome sedimentation experiments, we observed protection
257 from H-D exchange in the PAT domain and 11-mer repeats using 4ME-PC/PE and
258 DOPC/PE/DAG liposomes, with the magnitude and duration of H-D exchange protection in these
259 regions correlating with the observed fraction of PLIN3 bound in liposome sedimentation assays
260 **(Fig. S4B, 1D and 1G)**.
261
262 In contrast, with the 4ME-PC/PE and DOPC/PE/DAG lipid compositions, the 4-helix bundle did
263 not display large increases in deuterium exchange indicating that 4-helix bundle is not involved in
264 membrane binding in the absence of PA. Taken together, these results confirm that the PAT
265 domain and 11-mer repeats are the major lipid interacting regions of PLIN3, and that the 4-helix
266 bundle forms a stable tertiary structure that in general does not contribute to membrane
267 association, unless PA is present in membrane areas with shallow lipid packing defects. This
268 condition is particularly fulfilled at nascent LD formation sites.
269

270 **An expanded PAT domain binds DAG enriched membranes**

271 Our results suggested a role for the PAT domain in PLIN3 membrane association. However,
272 several studies [30, 31] have previously established the 11-mer repeats of PLINs are sufficient
273 for membrane binding, and to our knowledge, the PAT domain alone has not been demonstrated
274 to bind membranes. Complicating matters, the precise boundaries of the PAT domain have been
275 difficult to establish. Previous studies have suggested the PAT domain consists of the N-terminal
276 97 residues in PLIN3 [30], which are highly conserved with other PLINs **(Fig. 3A)**. However, high
277 sequence conservation between PLINs continues beyond residue 97 and ends at residue 115 in
278 PLIN3 **(Fig. 3A)**. This suggests the PAT domain may be larger than previously expected.
279 Consistent with the sequence conservation, both Alphafold [57] and RoseTTA fold [58] predict a
280 triangular alpha helical tertiary structure for the PAT domain that encompasses residues 22-116
281 **(Fig. 3B)**.
282
283 To investigate the PAT domain boundaries and membrane interaction capabilities, we purified
284 several C-terminal extended PAT domain constructs and the corresponding 11-mer repeats
285 counterparts **(Fig. 3C)** and assessed the ability of these fragments to bind DO liposomes
286 containing either 20mol% PA or 20mol% DAG. As an important note, we were unable to purify
287 the previously suggested PAT domain construct (residues 1-97), as this construct was not stably
288 expressed in *Escherichia coli*. This is consistent with the poor expression of the PAT domain of
289 PLIN1 in yeast [30].
290
291 In general, fragments encompassing the PAT domain bound strongly to liposomes in the
292 presence of DAG, with modest liposome binding in the presence of PA **(Fig. 3D)**. In contrast, the
293 11-mer repeats bound to liposomes containing either PA or DAG **(Fig. 3D)**. Taken together, the
294 data suggests that the PAT region does form a domain that spans residues 22-116 in PLIN3.
295 Notably, this expanded PAT domain is capable of membrane binding and displays a preference
296 for binding DAG enriched membranes, while the 11-mer repeats of PLIN3 do not.
297

298 **Conformational Rearrangements of the PAT Domain upon Membrane Binding**

299 We first sought to confirm the effects of liposome binding on secondary structure of PLIN3 by
300 circular dichroism (CD) **(Fig. S5)**. Liposomes were prepared with 4ME-PC/PE/PA, which recruited
301 all the PLIN3 constructs (full length, PAT, 11-mer repeats, PAT/11-mer repeats, 4-helix bundle)
302 in the previous liposome co-sedimentation experiments. For full length PLIN3, the presence of

303 liposomes increased overall helicity as observed by an increased negative peak around 222nm
304 in the CD spectra. In comparison, the CD spectra of the 4-helix bundle was largely unaffected by
305 the presence of liposomes and was consistent with a stable alpha helical structure. In contrast,
306 the PAT/11-mer repeats adopted a mostly random coil structure in solution with a negative peak
307 around 200nm, and a shift to alpha helices in the presence of liposomes as indicated by a large
308 negative peak at 222nm. Liposomes induced similar changes in the CD spectra for both the PAT
309 domain and 11-mer repeats alone. Taken together, this confirms that the increase in helicity
310 observed in full length PLIN3 by membranes was due to the PAT/11-mer repeats undergoing a
311 disorder/alpha helical transition. This is in line with our HDX-MS results and prior studies of PLIN2
312 and PLIN3 fragments [55, 59].
313
314 Next, to investigate if membranes induced conformational changes in the PAT domain, we applied
315 the pulsed-dipolar spectroscopy (PDS) technique of double electron-electron resonance (DEER)
316 [60, 61] to full length PLIN3 in solution and bound to liposomes. PDS is a collection of several,
317 based on recording electron spin-echo (ESE), pulse ESR techniques [62-66] routinely applied to
318 characterize protein conformations by providing accurate constraints in the distance range of ~10-
319 90Å. The amplitude of detected ESE depends on dipolar coupling between the spins of unpaired
320 electrons in nitroxide spin labels covalently bound to engineered cysteine residues. Stepping out
321 pulse separation in the sequence produces the time domain ESE envelope, from which the
322 distances could be reconstructed. [62-65].
323
324 Two sets of residues (25 and 96; 37 and 114) were selected for spin labeling, which were
325 respectively 71 and 77 residues apart in the primary sequence but predicted to be in close
326 proximity by AlphaFold and RoseTTAFold **(Fig. 4A-4C)**. Comparison of the DEER decoherence
327 (decay) times indicated that the PAT domain is less structured and/or intrinsically disordered in
328 solution versus when bound to liposomes, which is consistent with our HDX-MS and CD analysis
329 **(Fig. 4D)**. One can estimate, based on ~20% extent of decay in solution compared to liposomes
330 that the decoherence time is of the order of 20μs, which corresponds to nearly a 100Å separation
331 expected for a random polypeptide chain with stiffness [67]. In contrast, with liposomes the
332 decoherence times are fast enough to decay to background well within the evolution time of 1.2
333 μs used in the liposome DEER measurements. The decays do not show oscillations, as is
334 frequently observed for spin pairs with narrow distance distributions [68-71]. As a control to rule

335 out lateral aggregation [69], we attached a single spin-label to residue 37C and did not observe a
336 dipolar evolution (DEER shape) that could indicate a pair with a shorter than ~80Å separation
337 based on only slightly concave shape of the signal **(Fig. 4E)**. The DEER data thus suggest that
338 conspicuous dipolar signals in the doubly labeled proteins result from intramolecular interactions,
339 rather than being caused by intermolecular interactions on membranes.
340
341 Distance distributions could be obtained in the presence of liposomes. The results showed semi-
342 broad distance spreads of ~20-40Å for the 25C/96C pair and ~20-35Å for the 37C/114C pair **(Fig.**
343 **4F, 4G)**. These distances are comparable but do not exactly match the simulated distances using
344 the AlphaFold and RoseTTAFold structure predictions that have only modest confidence levels
345 **(Fig. 4A)** [57, 58]. For comparison, an extended alpha helix would result in distances of ~100Å
346 for these two sites. We also checked the spectral shape by recording field-swept echo with pulse
347 separation of 250ns and did not notice any conspicuous broadening that could indicate a shorter
348 range of distances (<15Å). We do however see from continuous wave (CW) ESR of 37C/114C
349 **(Fig. S6)** that there might be a sizeable fraction of spins in the 15-20Å range whose contribution
350 to the distance distribution will be significantly attenuated, since DEER has low sensitivity to
351 distances in this range. The conformations with this distance range correlate well with AlphaFold
352 predictions. The spread of the P(r) to longer distances could originate from the mobility of the C-
353 terminal helix where residue 114C is located **(Fig. 4C)**. Taken together, we concluded that the
354 PAT domain does form a folded domain when bound to membranes and this domain is likely
355 mobile with a structure similar but not identical to the AlphaFold and RoseTTAFold predictions.
356
357 **DAG recruits PLIN3 to membrane bilayers and droplets in vitro**
358 To verify a role for the PAT domain in DAG binding, we conducted an independent set of
359 experiments to test if purified PLIN3 with GFP fused to the N-terminus bound DAG enriched
360 membranes using droplet embedded vesicles (DEVs) [7, 35, 45, 72]. DEVs have emerged as a
361 powerful in vitro system to model emerging LDs that bud from membrane bilayers. A major
362 advantage of DEVs is the ability to not only monitor membrane association, but to also examine
363 the protein distribution and preference for droplet monolayers versus membrane bilayers.
364
365 DEVs were generated by adding the neutral lipids TAG or DAG to giant unilamellar vesicles
366 (GUVs) of DOPC that were marked with fluorescent phospholipids **(Fig. 5A)**. As observed
367 previously [45, 73], full length PLIN3 was strongly recruited to the monolayer surface of triolein

368 droplets with almost no bilayer signal **(Fig. 5B, 5D)**. Addition of diolein (DO-DAG) generated small
369 droplet buds, and full length PLIN3 was recruited equally to the droplet and bilayer surface **(Fig.**
370 **5C, 5D)**. Residues 1-204 of PLIN3 that contained both the PAT domain and 11-mer repeats
371 behaved nearly identical to full length PLIN3 in both TAG and DAG containing DEVs **(Fig. 5B, 5C**
372 **and 5E)**.
373
374 Next, we tested fragments of the PAT domain and 11-mer repeats using both triolein and diolein
375 DEVs. The 11-mer repeats preferentially bound the droplet surface of triolein DEVs with the
376 magnitude of signal dependent on the length of the 11-mer repeats **(Fig. 5B, 5G and 5I)**. In
377 contrast, PAT domain fragments did not bind to the droplet or bilayer surface of triolein DEVs **(Fig.**
378 **5B, 5F and 5H)**. The PAT domain was recruited to diolein DEVs, and the largest fragment
379 (residues 1-116) bound to both the droplet and bilayer surface with similar magnitudes to full
380 length PLIN3 **(Fig. 5C, 5F and 5H)**. The 11-mer repeats also bound to both the droplet and bilayer
381 surface of diolein DEVs, but to a lesser extent **(Fig. 5C, 5G and 5I)**. These results are consistent
382 with our previous hypothesis that the PAT domain is larger than previously expected and that this
383 functional PAT domain binds DAG enriched membranes, while the 11-mer repeats can also bind
384 DAG enriched membranes but display a preference for TAG containing droplets over membrane
385 bilayers.
386
387 **DAG accumulation is sufficient to recruit PLIN3 to the ER in cells**
388 DAG has previously been proposed to recruit PLIN3 to the ER in cells by blocking its hydrolysis
389 or acylation or by the exogenous addition of DAG [74]. This is consistent with the current model
390 for LD formation, where DAG accumulates at the site of TAG nucleation on the ER membrane
391 [18, 19, 75], the local high concentration of neutral lipids promotes LD nucleation through seipin
392 [15], and cytoplasmic PLIN3 marks these sites [10, 49]. We sought to test whether DAG
393 accumulation was sufficient for PLIN3 recruitment using an independent system and also assess
394 what fragments of PLIN3 were necessary and sufficient for ER recruitment.
395
396 To best visualize PLIN3 recruitment to ER membranes, we generated intracellular giant ER
397 vesicles (GERVs) by submitting cells to hypotonic medium [72, 76, 77] **(Fig. 6A)**. After exchange
398 to hypotonic medium, cells were pretreated with DMSO or the DGAT inhibitors (DGATi), followed
399 by oleic acid to induce TAG or DAG synthesis [77] **(Fig. 6A)**. Confocal microscopy was used to

400 visualize cells prior and after exchange to hypotonic medium, and after oleic acid treatment.
401 Imaging was done in the following minutes after the treatments.
402
403 As expected, the majority of subcellular localization of GFP-tagged PLIN3 was cytoplasmic in
404 both normal and hypotonic media without addition of oleic acid **(Fig. 6B, upper panels)**, and co-
405 localized with LDs **(Fig. 6D)**. Under conditions of DGAT inhibition, PLIN3 co-localized to the outer
406 periphery of GERVs **(Fig. 6B, yellow arrow, 6E and 6F)**, which suggests DO-DAG accumulation
407 is sufficient to recruit PLIN3 to ER membrane bilayers.
408
409 In line with our previous results, a construct containing both the PAT domain and 11-mer repeats
410 showed a similar subcellular localization as full length PLIN3 under all conditions **(Fig. 6C-6F)**.
411 This suggests the PAT domain and 11-mer repeats are sufficient for PLIN3 recruitment to both
412 DAG enriched membrane bilayers and TAG containing LDs, which might also contain DAG whose
413 concentration could increase the protein binding level. Interestingly, constructs containing only
414 the PAT domain (residues 1-116) or only the 11-mer repeats (residues 114-204), which bound to
415 DEVs in a DAG-dependent manner, remained cytoplasmic under all conditions **(Fig. 6D, 6E, S7)**.
416 Taken together, we concluded that PLIN3 is capable of binding both DAG enriched ER
417 membranes and early LDs, and that the PAT domain and 11-mer repeats are both necessary and
418 synergize to perform these functions in cells.
419
420

421 **DISCUSSION**

422 Here we find that PLIN3 not only binds LDs, but also membrane bilayers enriched in DAG and
423 PA. These results are in line with other studies that revealed PLIN3 binding to DAG [74, 78, 79].
424 In our hands, DAG binding was observed with multiple in vitro systems (e.g. liposomes, DEVs)
425 and DAG was also sufficient for PLIN3 recruitment to the ER in cells. Cellular recruitment to
426 membranes by DAG is consistent with a seminal study that used inhibitors to block DAG
427 hydrolysis or acylation and exogenous DAG to promote ER recruitment of PLIN3 [74].
428 Independent experiments in yeast have also demonstrated that membrane-anchored PLIN3 is
429 sufficient to bind to DAG enriched subdomains in the ER [78, 79]. Here we show that oleate
430 addition in combination with DGAT inhibition is sufficient for the subcellular redistribution of PLIN3
431 to the ER, which mimics normal the LD biogenesis pathway.
432
433 There are several mechanistic implications of PLIN3 recruitment to DAG enriched membranes.
434 First, this implies that PLIN3 is recruited to sites of LD formation, not only through TAG generation,
435 but also at the initial stages when DAG begins to accumulate. This raises a likely possibility that
436 PLIN3 may play an active role in the early stages of LD formation by stabilizing DAG enriched
437 regions on ER [78], and define sites of LD formation, before or in concomitant with seipin. Once
438 PLIN3 binds to accumulated DAG, it might coat the curved surface of a growing DAG/TAG lens
439 and regulate LD budding, in conjunction with seipin.
440
441 PA is another TAG precursor that is present at sites where LD originate [17] and can bind to seipin
442 [16]. In addition to DAG, it was found to have a significant impact on the recruitment of PLIN3 to
443 membranes in vitro. Thus, it may increase the translocation of PLIN3 to early LD formation sites.
444 These two TAG precursors appear to provide specificity for the association of PLIN3 with
445 membranes. From a curvature standpoint, DAG has a more negative curvature compared to PA
446 and PE, whereas PE has a more negative curvature than PA [80]. This suggests that membrane
447 curvature cannot solely account for the major role of PA in PLIN3 membrane binding specificity.
448 However, from a surface charge perspective, PA and PE together may act synergistically by
449 increasing charge of PA on the membrane [46, 81, 82]. In this scenario, PLIN3 recruitment to LD
450 nucleation sites could be enhanced by specific recognition of PA, potentially through the 4-helix
451 bundle. Therefore, PLIN3 membrane association may not only be determined by membrane
452 packing defects, but could also involve selective physical interactions between PLIN3 and DAG

453 or PA. This idea is also supported by a previous study that found that the LD binding properties
454 of PLINs are sensitive to the polar residue composition of their amphipathic helices [83].
455
456 In this study, we attempted to clarify the function and boundaries of the PAT domain. Our HDX-
457 MS results using full length PLIN3 clearly implicate both the PAT domain and 11-mer repeats in
458 membrane binding. In addition, we were able to define a functional PAT domain that
459 encompasses all of the conserved residues within PLINs and is longer than previously suggested.
460 This expanded PLIN3 PAT domain is sufficient to bind DAG enriched membranes, but not LDs.
461 In contrast, the 11-mer repeats display some affinity for DAG enriched membranes and are
462 necessary to bind LD monolayers. Our overall conclusion is that the PAT domain and 11-mer
463 repeats serve synergistic functions, as the individual regions are necessary for both LD and DAG
464 recruitment in cells.
465
466 The PAT domain is predicted to adopt a triangular tertiary structure by both AlphaFold and
467 RoseTTAFold. The DEER distance measurements and CW ESR data are not identical to these
468 predictions, but do indicate that when bound to membranes the PAT domain adopts a folded
469 domain. This conclusion is supported by our HDX-MS results that found the peptides within the
470 PAT domain display longer protection times from H-D exchange, which could be due to either a
471 tertiary structure more resistant to unfolding or a longer membrane residency time. We note that
472 the membrane bound PAT domain structure is likely dynamic and additional distance
473 measurements at distinct sites are needed to verify the accuracy of the predicted triangular
474 structures.
475
476 To our knowledge, our finding that the PAT domain of PLIN3 is sufficient to bind DAG represents
477 the first functional role for the PAT domain in any PLIN. This suggests that the highly conserved
478 PAT domain in other PLINs may serve similar or related functions. For example, could the PAT
479 domain be a general sensor for DAG in membrane bilayers? Or could the PAT domain of other
480 PLINs potentially bind to other neutral lipids (e.g. CEs, TAGs, retinol esters)? Given the previously
481 observed differing neutral lipid preference of PLINs [20] and the involvement of the PAT domain
482 in lipid/membrane binding, this now raises the questions if this is due to the PAT domain
483 preference, the 11-mer repeat preference, or the synergistic action of the combined PAT/11-mer
484 repeat units.
485

Lastly, our results are consistent with previous studies that found the PLIN3 4-helix bundle does not bind LDs, but other PLINs 4-helix bundles can bind LDs [33]. While the domain boundaries of the 4-helix bundles seem reasonable given structure of mouse PLIN3 [54], the variable membrane binding affinities we observed for the PAT domain and 11-mer repeats does raise the question if stability of 4-helix bundle, and consequently the ability to unfold and bind membranes or LDs in other PLINs may depend on the domain boundaries of specific constructs. Thus, we suggest it is reasonable to revisit the ability of the 4-helix bundles from other PLINs using constructs that can be stably purified in vitro to rule out potential artifacts from the use of unstable 4-helix bundles.

496 **MATERIALS AND METHODS**

497 **Protein expression and purification**

498 The genes encoding PLIN3 constructs were codon-optimized for expression in *Escherichia coli*
499 and cloned into pTHT, which is a derivative of pET28 that contains a TEV cleavable N-terminal
500 6x His tag. For GFP tagged PLIN3 constructs, monomeric superfolder GFP (msfGFP) was
501 inserted between the 6x His tag and the N-terminus of PLIN3. PLIN3 plasmids were transformed
502 into BL21(DE3) RIPL cells and protein expression was induced with 1mM isopropyl β-D-1-
503 thiogalactopyranoside (IPTG) at 37°C for 3h. Cells was harvested by centrifugation at 3,320 x g
504 for 20mins and stored at -80°C until use. Cell pellets were resuspended with buffer A containing
505 500mM NaCl, 20 mM Tris-HCl pH 7.5, 5% glycerol, 5mM 2-mercaptoethanol (BME) and lysed by
506 sonication. Cell lysates were centrifuged at 81,770 x g for 1h at 4°C and the resulting supernatant
507 was incubated with 5mL of Ni-NTA resin for 2h at 4°C prior to loading onto a gravity column. The
508 Ni-NTA resin was washed with buffer B containing 500mM NaCl, 20mM Tris-HCl pH 7.5, 5%
509 glycerol, 5mM BME and 60mM imidazole. Human PLIN3 proteins were eluted with buffer C
510 containing 500mM NaCl, 20mM Tris-HCl pH 7.5, 5% glycerol, 5mM BME and 300mM imidazole.
511 Eluted protein was applied to a HiLoad 26/600 Superdex 200 pg column (GE life sciences)
512 equilibrated with 150mM NaCl, 20mM Tris-HCl pH 7.5, 5% glycerol, and 5mM BME. The average
513 yield of full length PLIN3, PAT/11-mer repeats and 4-helix bundle throughout expression and
514 purification was between 5-10mg from a 1L culture of *Escherichia coli.* The yield of PAT or 11-
515 mer repeats constructs or GFP tagged PLIN3 fragments was ~1mg/L. Protein was analyzed by
516 SDS-PAGE, concentrated using a centrifugal tube (10K MWCO, Pall Corporation), aliquoted and
517 stored at -80°C.

518

519 **Lipids**

520 The following lipids were purchased from Avanti Polar Lipids: 1,2-dioleoyl-sn-glycero-3-
521 phosphocholine (DOPC, catalog #850375), 1,2-dioleoyl-sn-glycero-3-phosphoethanolamine
522 (DOPE, catalog #850725), 1,2-dioleoyl-sn-glycero-3-phosphate (DOPA, catalog #840875), 1,2-
523 dioleoyl-sn-glycero-3-phospho-L-serine (DOPS, catalog #840035), 1-palmitoyl-2-oleoyl-glycero-
524 3-phosphocholine (POPC, catalog #850457), 1-palmitoyl-2-oleoyl-sn-glycero-3-
525 phosphoethanolamine (POPE, catalog #850757), 1-palmitoyl-2-oleoyl-sn-glycero-3-phosphate
526 (POPA, catalog #840857), 1-palmitoyl-2-oleoyl-sn-glycero-3-phospho-L-serine (POPS, catalog
527 #840034), 1,2-diphytanoyl-sn-glycero-3-phosphocholine (4ME-PC, catalog #850356), 1,2-

528 diphytanoyl-sn-glycero-3-phosphoethanolamine (4ME-PE, catalog #850402), 1,2-diphytanoyl-sn-
529 glycero-3-phosphate (4ME-PA, catalog #850406), 1,2-diphytanoyl-sn-glycero-3-phospho-L-
530 serine (4ME-PS, catalog #850408), 1-palmitoyl-2-oleoyl-sn-glycerol (DAG, catalog #800815), L-
531 α-phosphatidylinositol (Soy PI, catalog #84044), L-α-phosphatidylinositol-4-phosphate (Brain,
532 Porcine (PI(4)P, catalog #840045), N-stearoyl-D-erythro-sphingosine (C18:1 ceramide, catalog
533 #860518). 1,2,3-Trioleoyl Glycerol was purchase from Cayman Chemicals (TAG, catalog #26950).
534
535 **Liposome co-sedimentation assay**
536 To prepare liposomes, lipids were dried under a nitrogen gas stream and dissolved with buffer
537 containing 50mM NaCl and 50mM HEPES pH 8.0 with a total lipid concentration of 2mM, unless
538 otherwise noted. Liposomes were generated by repeated cycles of flash freezing in liquid nitrogen,
539 thawing in 37°C water bath, and vortexing [84]. Liposomes were characterized using dynamic
540 light scattering and showed uniform distribution for most lipid compositions. Lamellarity analysis
541 of liposomes was not carried out, but liposomes likely contained a mixture of multi-lamellar
542 vesicles and unilamellar vesicles. For liposome co-sedimentation assays, 20 μL of 12μM purified
543 protein was incubated with 40μL of 2 mM liposomes for 40mins at 23°C. Protein fractions bound
544 to liposomes were isolated by centrifugation at 100,000 x g for 70mins at 4°C and analyzed by
545 SDS-PAGE.
546
547 **Circular Dichroism**
548 Circular dichroism (CD) spectra of purified PLIN3 full length and its constructs were measured on
549 Spectropolarimeter (Jasco, J-715). 0.12~0.24mg/ml of protein was incubated with 1~2mM
550 liposomes containing 4ME-PC/PE/PA for 40mins prior to measurement. Liposomes/protein
551 mixture was prepared in the buffer containing 20mM Tris pH 7.5 and 150mM NaCl. CD spectra
552 was measured between 190nm and 260nm in increments of 1nm, with a bandwidth of 50nm and
553 an averaging time of 1min at 25°C. 10 iterations of spectra were averaged and was reported into
554 a mDeg, which was converted to molar ellipticity (m°*M/(10*L*C) of which unit is expressed in
555 degree cm^2 $dmol^{-1}$. Molar ellipticity of each protein fragments in the absence or presence were
556 plotted using GraphPad prism software. Comparisons of spectra in the presence and the absence
557 of liposome were assessed using unpaired *t* test with $p<0.05$ of statistical significance.
558
559 **Artificial lipid droplet flotation assay**

560 Artificial lipid droplets (ALDs) were prepared by mixing phospholipids and triacylglycerols (TAGs).
561 Di-oleoyl phospholipids were dried under a nitrogen gas stream. Dried lipids were resuspended
562 with lipid droplet flotation assay buffer containing 50mM NaCl and 50mM HEPES pH 8.0 and
563 TAGs in the molar ratio of 2:5. ALDs were formed by repeating the cycles of vortex for 10sec and
564 rest for 10sec. ALDs were further vortexed before use for the assay. 100μL of ALDs were mixed
565 with 5μL of human PLIN3 and 105μL of lipid flotation assay buffer to give a final concentration of
566 5μM protein and 1.5mM phospholipids. The average diameters of different ALDs were measured
567 by dynamic light scattering (DLS). The concentration of ALDs were determined by optical density
568 at 600nm. The mixture of human PLIN3 and ALDs was incubated for 1h at 23°C. To generate a
569 sucrose gradient, 140μL of a 75% sucrose solution was added to 210μL of the protein-ALD
570 mixture to give a final concentration of 30% sucrose. The resulting mixture (320μL) was
571 transferred to an ultra-centrifuge tube. 260μL of a 25% sucrose solution was applied on top of 30%
572 sucrose/protein/ALDs mixture. Lastly, 60μL of lipid flotation assay buffer was laid on the top. ALDs
573 were floated by centrifugation at 76,000 x g for 3h at 20°C with sucrose gradient of 30% (bottom),
574 25% (middle), and 0% (top). Three fractions of 100μL from the top, 260μL from the middle and
575 280μL from the bottom were collected and analyzed by SDS-PAGE.
576
577 **Hydrogen-Deuterium Exchange Mass Spectrometry (HDX-MS)**
578 *Sample preparation*
579 HDX reactions for PLIN3 deuterium pulse were conducted in a final reaction volume of 10μL with
580 a final concentration 2.12μM PLIN3. Exchange was carried out in triplicate for a single time point
581 (3 sec at 0 °C). Hydrogen deuterium exchange was initiated by the addition of 9μL of D2O buffer
582 solution (20mM HEPES pH 7.5, 100mM NaCl) to 1μL of protein, to give a final concentration of
583 84.9% D2O. Exchange was terminated by the addition of 60μL acidic quench buffer at a final
584 concentration 0.6M guanidine-HCl and 0.9% formic acid. Samples were immediately frozen in
585 liquid nitrogen at -80°C. Fully deuterated samples were generated by first denaturing the protein
586 in 3M guanidine for 1h at 20°C. Following denaturing, 9μL of D2O buffer was added to the 1μL of
587 denatured protein and allowed to incubate for 10mins at 20°C before quenching with 0.6M
588 guanidine-HCl and 0.9% formic acid. Samples were immediately frozen in liquid nitrogen at -80°C,
589 and all timepoints were created and run in triplicate.
590

591 HDX reactions comparing PLIN3 in the presence of PA liposomes (60mol% 4ME-PC, 20mol%
592 4ME-PE, 20mol% 4ME-PA) were conducted in a final reaction volume of 10μL with a final protein
593 concentration of 3μM and final liposome concentration of 1mM. Protein and liposomes were
594 preincubated together for 2mins at 20°C before the addition of 7μL D2O buffer solution (50mM
595 HEPES pH 8.0, 50mM NaCl) for a final concentration of 63% D2O. Exchange was carried out for
596 3sec, 30sec, 300sec and 3000sec, and exchange was terminated by the addition of 60μL acidic
597 quench buffer at a final concentration 0.6M guanidine-HCl and 0.9% formic acid. Samples were
598 immediately frozen in liquid nitrogen at -80°C, and all timepoints were created and run in triplicate.
599
600 HDX reactions comparing PLIN3 in the presence of two different liposomes (60mol% DOPC,
601 20mol% DOPE, 20mol% DAG liposomes and 80mol% 4ME-PC, 20mol% 4ME-PE liposomes)
602 were conducted in a final reaction volume of 10μL with a final protein concentration of 3μM and
603 final liposome concentration of 500μM. Protein and liposomes were preincubated together for
604 2mins at 20°C before the addition of 8μL D2O buffer solution (50mM HEPES pH 8.0, 50mM NaCl)
605 for a final concentration of 72% D2O. Exchange was carried out for 3sec, 30sec, 300sec and
606 3000sec, and exchange was terminated by the addition of 60μL acidic quench buffer at a final
607 concentration 0.6M guanidine-HCl and 0.9% formic acid. Samples were immediately frozen in
608 liquid nitrogen at -80°C, and all timepoints were created and run in triplicate.
609
610 *Protein digestion and MS/MS data collection*
611 Protein samples were rapidly thawed and injected onto an integrated fluidics system containing a
612 HDx-3 PAL liquid handling robot and climate-controlled (2°C) chromatography system (LEAP
613 Technologies), a Dionex Ultimate 3000 UHPLC system, as well as an Impact HD QTOF Mass
614 spectrometer (Bruker). The protein was run over either one (at 10°C) or two (at 10°C and 2°C)
615 immobilized pepsin columns (Trajan; ProDx protease column, 2.1mm x 30mm PDX.PP01-F32)
616 at 200μL/min for 3mins. The resulting peptides were collected and desalted on a C18 trap column
617 (Acquity UPLC BEH C18 1.7mm column (2.1 x 5mm); Waters 186003975). The trap was
618 subsequently eluted in line with an ACQUITY 1.7μm particle, 100 × 1mm2 C18 UPLC column
619 (Waters), using a gradient of 3-35% B (Buffer A 0.1% formic acid; Buffer B 100% acetonitrile) over
620 11mins immediately followed by a gradient of 35-80% over 5mins. Mass spectrometry
621 experiments acquired over a mass range from 150 to 2200m/z using an electrospray ionization
622 source operated at a temperature of 200°C and a spray voltage of 4.5kV.

623

624 *Peptide identification*

625 Peptides were identified from the non-deuterated samples of PLIN3 using data-dependent
626 acquisition following tandem MS/MS experiments (0.5sec precursor scan from 150-2000m/z;
627 twelve 0.25sec fragment scans from 150-2000m/z). MS/MS datasets were analyzed using
628 PEAKS7 (PEAKS), and peptide identification was carried out by using a false discovery based
629 approach, with a threshold set to 1% using a database of known contaminants found in Sf9 and
630 E. coli cells [85]. The search parameters were set with a precursor tolerance of 20ppm, fragment
631 mass error 0.02 Da, charge states from 1-8, leading to a selection criterion of peptides that had -
632 10logP scores of 22.8 for the pulse experiment and 20.9 for the liposome experiment.

633

634 *Mass Analysis of Peptide Centroids and Measurement of Deuterium Incorporation*

635 HD-Examiner Software (Sierra Analytics) was used to automatically calculate the level of
636 deuterium incorporation into each peptide. All peptides were manually inspected for correct
637 charge state, correct retention time, appropriate selection of isotopic distribution, etc. Deuteration
638 levels were calculated using the centroid of the experimental isotope clusters. Results are
639 presented as relative levels of deuterium incorporation, with the only correction being applied
640 correcting for the deuterium oxide percentage of the buffer utilized in the exchange (63% and
641 72%). For the experiment with a fully deuterated sample, corrections for back exchange were
642 made by dividing the pulse %D value by the fully deuterated %D value and multiplying by 100.
643 The raw %D incorporation for the fully deuterated sample is included in the source data, with the
644 average back exchange being 33%, and ranging from 10-60%. Differences in exchange in a
645 peptide were considered significant if they met all three of the following criteria: : ≥5% change in
646 exchange and ≥0.4 Da difference in exchange. The raw HDX data are shown in two different
647 formats. Samples were only compared within a single experiment and were never compared to
648 experiments completed at a different time with a different final D2O level. The data analysis
649 statistics for all HDX-MS experiments are in Supplemental Table 1 according to the guidelines of
650 [86]. The mass spectrometry proteomics data have been deposited to the ProteomeXchange
651 Consortium via the PRIDE partner repository with the dataset identifier PXD025717 [87].

652

653 **Dynamic light scattering**

654 The size of liposomes was measured by dynamic light scattering (Brookhaven Instruments
655 NanoBrook Omni), with or without full length PLIN3. Liposomes were prepared in the buffer
656 containing 50mM HEPES pH 8.0 and 50mM NaCl by repeating the freeze/thaw cycles to prevent
657 multilamellar vesicle formation. Each protein construct was incubated with liposomes in 1:200 of
658 molar ratio at 25°C for 40mins. DLS was conducted using a scattering angle of 90°, and the
659 liposome/protein mixture was equilibrated for 5mins after loading into the instrument to get a
660 uniform temperature and minimize any loading effects prior to measurement. The number
661 average size distribution (%) was considered as a relative concentration of particles with a certain
662 size. For analysis, measurements with large outlier peaks, which were suspected to be due to the
663 dust particles or aggregated vesicles, were discarded, and three runs that did not contain outlier
664 peaks were used for the data analysis. The mode of the distribution (e.g., the size having the
665 highest peak in the number average size distribution) was chosen from each of these three
666 measurements and averaged to obtain the reported average diameter. A representative size
667 distribution is shown for each sample.
668
669 **Site-directed spin-labeling**
670 Recombinant PLIN3 cysteine-substituted proteins were purified using Ni-NTA resin in a buffer
671 500mM NaCl, 20mM Tris pH 7.5, 5% glycerol and eluted in a buffer of 500mM NaCl, 20mM Tris
672 pH 7.5, 5% Glycerol, 300mM imidazole. Elution was spin-labeled with 1μg/mL (S-(1-oxyl-2,2,5,5-
673 tetramethyl-2,5-dihydro-1H-pyrrol-3-yl) methyl methanesulfonothioate), MTSL, (Santa Cruz
674 Biotech) dissolved in acetonitrile at 4°C overnight. The spin-labeled proteins were further purified
675 by HiLoad 26/600 Superdex 200 pg column (GE life sciences) in a buffer of 150mM NaCl, 20mM
676 Tris pH 7.5 to remove unreacted spin labels.
677
678 **Sample preparations for DEER spectroscopy**
679 Protein samples in solutions were prepared at ca. 40-60μM concentrations in 20mM Tris at pH
680 7.5, 150mM NaCl, and 40% glycerol. Liposome samples containing 10μM protein and 3.33 mM
681 lipid were prepared by mixing 30μM protein stocks with 5mM liposome solutions using 1 to 2
682 aliquots followed by 30mins incubation at room temperature. The liposomes were freshly
683 prepared by rehydration of lyophilized 80/20 mol% 4ME-PC/PE followed by seven freeze/thaw
684 cycles. Freshly-prepared 20μL of spin-labeled samples were loaded into 1.8mm inner diameter

685 Pyrex sample tubes (Wilmad-LabGlass), frozen by plunging in liquid nitrogen, and stored in liquid
686 nitrogen for PDS measurements.
687
688 **DEER data collection and analysis**
689 PDS DEER measurements were performed at 60K with a home-built Ku band pulse ESR
690 spectrometer operating around 17.3GHz [64, 88]. A four-pulse DEER sequence [89] was
691 employed using for spin-echo detection $\pi/2$- and π-pulses with respective widths of 16 and 32ns,
692 the π-pulse for pumping was 16ns. The detection frequency matched the peak at the low-field
693 spectral edge, while pumping was performed at a lower by 70MHz frequency, corresponding to
694 the central maximum. A 32-step phase cycle [90] was applied to suppress unwanted contributions
695 to the signal. Nuclear electron spin-echo envelope modulation (ESEEM) caused by surrounding
696 protons was suppressed using the data from four measurements. In this method the initial pulse
697 separations and the start of detection were advanced by 9.5ns in subsequent measurements, i.e.
698 by the quarter period of the 26.2MHz nuclear Zeeman frequency for protons at 0.615T
699 corresponding to the working frequency. The four signal traces were summed to achieve deep
700 suppression of nuclear ESEEM, [91].
701
702 The solution samples had phase memory times, T_m's, of about 2.5μs, so the data could be
703 recorded up to 3μs evolution time (t_m). Such evolution times did not provide sufficient decay of
704 the dipolar coherence to the background level, providing however clear indication of unstructured
705 nature of the protein in solution. Any residual secondary structure could be probed by using
706 multiple labeling sites, however other techniques did not encourage this undertaking. For
707 solutions the DEER data were acquired in less than 12h. Faster phase relaxation times (~1μs)
708 and low spin concentrations in liposome samples required signal averaging for ~24h to facilitate
709 good reconstruction by Tikhonov regularization. [92, 93]
710
711 For liposomes, time domain DEER data, $V(t)$, were recorded and preprocessed using standard
712 approaches [62, 65, 89, 94] before their reconstruction into distance distributions, $P(r)$'s. The first
713 step is to remove signal decay caused by intermolecular dipole-dipole couplings, followed by
714 subtracting the residual background from the spins whose partner was not flipped by the pump or
715 missing. This was done, as usual, by fitting the latter points (about a half of the record) of $\ln[V(t)]$
716 to a low-order polynomial, usually a straight line for solutions (and often for liposomes),

717 extrapolating it to zero time, and subtracting out from ln[$V(t)$]; so that the antilog yields $u(t) = d(t)$
718 + 1. Here $d(t)$ is the dipolar evolution representing part. Once $u(t)$ is normalized as $u(t)/u(0)$, it
719 serves as a typical form of DEER data presentation, while $v(t)=(u(t)-1)/u(0)$, gives background-
720 free "dipolar" data to be converted to a distance distribution between spins in pairs. We used L-
721 curve Tikhonov regularization [92] for distance reconstruction. The Tikhonov regularization utility
722 allowed selection of either the signal or its derivatives in the Tikhonov functional and selection of
723 the regularization parameter. The latter increases $P(r)$ smoothness at the expense of introducing
724 some broadening.
725
726 Dipolar signal amplitude ("modulation depth") is given by $v(0)$. This would be accurate to the extent
727 the background or $V(\infty)$, the asymptotic value of $V(t)$, is known. This depth, tabulated by
728 calculations for typical pulse sequence setup and verified in numerous experiments, is a measure
729 of a fraction of spins in pairs or oligomers [69, 95, 96]. It is thus useful in estimate of spin-labeling
730 efficiency and protein concentration.
731
732 **Cell culture**
733 Cos7 cells were maintained in Dulbecco's modified Eagle's medium (DMEM) supplemented with
734 10% heat inactivated fetal bovine serum (Life Technologies), 4.5gL^{-1} D-glucose, 0.1gL^{-1} sodium
735 pyruvate (Life Technologies) and 1% penicillin-streptomycin (Life Technologies). The cells were
736 cultured at 37°C under a 5% CO2 atmosphere.
737
738 **Transfection**
739 When indicated, Cos7 cells (60–70% confluence) plated into a 35mm cell-culture Mattek dishes
740 (with a glass coverslip at the bottom), (MatTek Corp. Ashland, MA). were transfected with 3μg of
741 plasmid DNA/ml using Polyethylenimine HCl MAX (Polysciences) following the manufacturer's
742 instructions. For co-expressions, RFP-KDEL or GFP-Plin3 constructs in equal concentrations
743 (1.5–2μg for each one) were transfected to cells 24h prior observation.
744
745 **Giant unilamellar vesicles, GUVs**
746 GUVs were prepared by electroformation following the protocol described in [97]. Phospholipids,
747 dioleoyl phosphatidylcholine (PC) (70%) and dioleoyl phosphatidylethanolamine (PE) (29%),
748 Rhodamine-DOPE 1% (w/w)), were purchased from Avanti Polar Lipids. The lipid mixture, in

749 chloroform at 0.5mM, was dried on an indium tin oxide (ITO)-coated glass plate. The lipid film was
750 desiccated for 1h. The chamber was sealed with another ITO- coated glass plate. The lipids were
751 then rehydrated with a sucrose solution (275mOsm). Electroformation was done using 100Hz AC
752 voltage at 1.0 to 1.4Vpp and maintained for at least 1h.
753
754 **Droplet-embedded vesicles (DEVs) preparation**
755 Artificial LDs (aLDs) were prepared in HKM buffer: 50mM HEPES, 120mM Kacetate, and 1mM
756 $MgCl_2$ (in Milli-Q water) at pH 7.4 and 275±15mOsm. To do so, 5μL of the lipid oil solution (triolein
757 or diacylglycerol purchased from Sigma) was added to 45mL of HKM buffer and the mixture was
758 sonicated as described in [98]. The resulting emulsion was then mixed with GUVs for five minutes
759 under rotator to generate DEVs [98]. DEVs were then placed on a glass coverslip pretreated with
760 10%(w/w) BSA and washed three times with buffer.
761
762 **Protein binding to DEVs**
763 For the protein binding experiments, 50μL HKM were deposited on the BSA-treated glass, 30μL
764 of the DEV solution added and 1.5μL purified PLIN3 or PLIN3 fragments added (in the case of
765 107-204 and 1-106 fragments, 3μL were added). The final protein concentration in the solution
766 was between 1μM to 4μM depending on the protein. For quantifications, 10-15 DEVs were
767 considered and the signal on the droplet and bilayer was determined by Fiji, via drawing 5-10
768 points-thick line profiles.
769
770 **Neutral lipid synthesis induction**
771 Wherever relevant, cells were exposed for 1h to 350μM oleic acid (OA) coupled to bovine serum
772 albumin (BSA) (0.2% weight/volume) to induce neutral lipids' synthesis. LipidTox DeepRed
773 (Thermo Fischer), was used to visualize lipid droplets or membranes enriched in neutral lipids.
774
775 **Giant Intra-Cellular ER vesicle experiments**
776 For GERV experiments, Cos7 cells were first transfected for 24h with the indicated eGFP
777 plasmids and RFP-KDEL. The culture media of the cells was next replaced by a hypotonic culture
778 media (DMEM:H2O, 1:20). The cells were then incubated at 37°C, 5% CO2 for 5mins, to induce
779 GERVs, and then they were visualized. Neutral lipids' synthesis was triggered by the addition of
780 OA and Z-stacks imaging of different entire cells was performed before and 15mins after OA

781 administration, as described in [77]. For the DGAT1 (Sigma, PF-04620110) and DGAT2 (Sigma,
782 PF-06424439) inhibitors used in Cos7, the dilution applied was 1/1000 for a final concentration of
783 3μg/mL. In the GERV protocol, the inhibitors were added to the cell medium before cell
784 transfection or during the hypotonic solution addition. The signal of PLIN3 or fragments thereof
785 was quantified for tens of GERVs by depicting the mean signal on the GERVs to which was
786 subtracted the bulk cytosolic signal; this resulted signal was normalized to the cytosolic signal.
787

788 **Structure prediction by AlphaFold and RoseTTAFold**

789 Structure prediction of PLIN3 was carried out by AlphaFold and RoseTTAFold. Two different
790 confidence values were generated (pLDDT from AlphaFold and rmsd from RoseTTAFold). These
791 values were converted using PHENIX to get relative confidence level from two softwares,
792 AlphaFold and RoseTTAFold [99].
793

794
795
796 **REFERENCES**
797

798 1. Thiam, A.R., R.V. Farese, Jr., and T.C. Walther, *The biophysics and cell biology of lipid*
799 *droplets.* Nat Rev Mol Cell Biol, 2013. **14**(12): p. 775-86.
800 2. Rubin, C.S., et al., *Development of hormone receptors and hormonal responsiveness in*
801 *vitro. Insulin receptors and insulin sensitivity in the preadipocyte and adipocyte forms of*
802 *3T3-L1 cells.* J Biol Chem, 1978. **253**(20): p. 7570-8.
803 3. Gibbons, G.F., K. Islam, and R.J. Pease, *Mobilisation of triacylglycerol stores.* Biochim
804 Biophys Acta, 2000. **1483**(1): p. 37-57.
805 4. Olzmann, J.A. and P. Carvalho, *Dynamics and functions of lipid droplets.* Nat Rev Mol Cell
806 Biol, 2019. **20**(3): p. 137-155.
807 5. Valm, A.M., et al., *Applying systems-level spectral imaging and analysis to reveal the*
808 *organelle interactome.* Nature, 2017. **546**(7656): p. 162-167.
809 6. Miyanari, Y., et al., *The lipid droplet is an important organelle for hepatitis C virus*
810 *production.* Nat Cell Biol, 2007. **9**(9): p. 1089-97.
811 7. Ben M'barek, K., et al., *ER Membrane Phospholipids and Surface Tension Control Cellular*
812 *Lipid Droplet Formation.* Dev Cell, 2017. **41**(6): p. 591-604 e7.
813 8. Choudhary, V., et al., *A conserved family of proteins facilitates nascent lipid droplet*
814 *budding from the ER.* J Cell Biol, 2015. **211**(2): p. 261-71.
815 9. Thiam, A.R. and L. Foret, *The physics of lipid droplet nucleation, growth and budding.*
816 Biochim Biophys Acta, 2016. **1861**(8 Pt A): p. 715-22.
817 10. Chung, J., et al., *LDAF1 and Seipin Form a Lipid Droplet Assembly Complex.* Dev Cell,
818 2019. **51**(5): p. 551-563 e7.

819 11. Gao, M., et al., *The biogenesis of lipid droplets: Lipids take center stage.* Prog Lipid Res,
820 2019. **75**: p. 100989.
821 12. Chorlay, A., et al., *Membrane Asymmetry Imposes Directionality on Lipid Droplet*
822 *Emergence from the ER.* Dev Cell, 2019. **50**(1): p. 25-42 e7.
823 13. Wang, H., et al., *Seipin is required for converting nascent to mature lipid droplets.* Elife,
824 2016. **5**.
825 14. Salo, V.T., et al., *Seipin regulates ER-lipid droplet contacts and cargo delivery.* EMBO J,
826 2016. **35**(24): p. 2699-2716.
827 15. Zoni, V., et al., *Pre-existing bilayer stresses modulate triglyceride accumulation in the ER*
828 *versus lipid droplets.* Elife, 2021. **10**.
829 16. Yan, R., et al., *Human SEIPIN Binds Anionic Phospholipids.* Dev Cell, 2018. **47**(2): p. 248-
830 256 e4.
831 17. Guyard, V., et al., *ORP5 and ORP8 orchestrate lipid droplet biogenesis and maintenance*
832 *at ER-mitochondria contact sites.* J Cell Biol, 2022. **221**(9).
833 18. Choudhary, V., et al., *Seipin and Nem1 establish discrete ER subdomains to initiate yeast*
834 *lipid droplet biogenesis.* J Cell Biol, 2020. **219**(7).
835 19. Choudhary, V., et al., *Architecture of Lipid Droplets in Endoplasmic Reticulum Is*
836 *Determined by Phospholipid Intrinsic Curvature.* Curr Biol, 2018. **28**(6): p. 915-926 e9.
837 20. Hsieh, K., et al., *Perilipin family members preferentially sequester to either*
838 *triacylglycerol-specific or cholesteryl-ester-specific intracellular lipid storage droplets.* J
839 Cell Sci, 2012. **125**(Pt 17): p. 4067-76.
840 21. Wolins, N.E., D.L. Brasaemle, and P.E. Bickel, *A proposed model of fat packaging by*
841 *exchangeable lipid droplet proteins.* FEBS Lett, 2006. **580**(23): p. 5484-91.
842 22. Brasaemle, D.L., *Thematic review series: adipocyte biology. The perilipin family of*
843 *structural lipid droplet proteins: stabilization of lipid droplets and control of lipolysis.* J
844 Lipid Res, 2007. **48**(12): p. 2547-59.
845 23. Greenberg, A.S., et al., *Perilipin, a major hormonally regulated adipocyte-specific*
846 *phosphoprotein associated with the periphery of lipid storage droplets.* J Biol Chem,
847 1991. **266**(17): p. 11341-6.
848 24. Jiang, H.P. and G. Serrero, *Isolation and characterization of a full-length cDNA coding for*
849 *an adipose differentiation-related protein.* Proc Natl Acad Sci U S A, 1992. **89**(17): p.
850 7856-60.
851 25. Diaz, E. and S.R. Pfeffer, *TIP47: a cargo selection device for mannose 6-phosphate*
852 *receptor trafficking.* Cell, 1998. **93**(3): p. 433-43.
853 26. Wolins, N.E., et al., *Adipocyte protein S3-12 coats nascent lipid droplets.* J Biol Chem,
854 2003. **278**(39): p. 37713-21.
855 27. Sztalryd, C. and D.L. Brasaemle, *The perilipin family of lipid droplet proteins: Gatekeepers*
856 *of intracellular lipolysis.* Biochim Biophys Acta Mol Cell Biol Lipids, 2017. **1862**(10 Pt B):
857 p. 1221-1232.
858 28. Wilson, M.H., S.C. Ekker, and S.A. Farber, *Imaging cytoplasmic lipid droplets in vivo with*
859 *fluorescent perilipin 2 and perilipin 3 knock-in zebrafish.* Elife, 2021. **10**.
860 29. Bulankina, A.V., et al., *TIP47 functions in the biogenesis of lipid droplets.* J Cell Biol, 2009.
861 **185**(4): p. 641-55.

862 30. Rowe, E.R., et al., *Conserved Amphipathic Helices Mediate Lipid Droplet Targeting of*
863 *Perilipins 1-3.* J Biol Chem, 2016. **291**(13): p. 6664-78.
864 31. Copic, A., et al., *A giant amphipathic helix from a perilipin that is adapted for coating*
865 *lipid droplets.* Nat Commun, 2018. **9**(1): p. 1332.
866 32. Mirheydari, M., et al., *Insertion of perilipin 3 into a glycero(phospho)lipid monolayer*
867 *depends on lipid headgroup and acyl chain species.* J Lipid Res, 2016. **57**(8): p. 1465-76.
868 33. Ajjaji, D., et al., *Dual binding motifs underpin the hierarchical association of perilipins1-3*
869 *with lipid droplets.* Mol Biol Cell, 2019. **30**(5): p. 703-716.
870 34. Bigay, J. and B. Antonny, *Curvature, lipid packing, and electrostatics of membrane*
871 *organelles: defining cellular territories in determining specificity.* Dev Cell, 2012. **23**(5): p.
872 886-95.
873 35. Chorlay, A. and A.R. Thiam, *Neutral lipids regulate amphipathic helix affinity for model*
874 *lipid droplets.* J Cell Biol, 2020. **219**(4).
875 36. Prevost, C., et al., *Mechanism and Determinants of Amphipathic Helix-Containing*
876 *Protein Targeting to Lipid Droplets.* Dev Cell, 2018. **44**(1): p. 73-86 e4.
877 37. Vamparys, L., et al., *Conical lipids in flat bilayers induce packing defects similar to that*
878 *induced by positive curvature.* Biophys J, 2013. **104**(3): p. 585-93.
879 38. Zhukovsky, M.A., et al., *Phosphatidic acid in membrane rearrangements.* FEBS Lett,
880 2019. **593**(17): p. 2428-2451.
881 39. Vanni, S., et al., *A sub-nanometre view of how membrane curvature and composition*
882 *modulate lipid packing and protein recruitment.* Nat Commun, 2014. **5**: p. 4916.
883 40. Fujimoto, Y., et al., *Long-chain fatty acids induce lipid droplet formation in a cultured*
884 *human hepatocyte in a manner dependent of Acyl-CoA synthetase.* Biol Pharm Bull,
885 2006. **29**(11): p. 2174-80.
886 41. Harayama, T. and H. Riezman, *Understanding the diversity of membrane lipid*
887 *composition.* Nat Rev Mol Cell Biol, 2018. **19**(5): p. 281-296.
888 42. Radhakrishnan, A., et al., *Switch-like control of SREBP-2 transport triggered by small*
889 *changes in ER cholesterol: a delicate balance.* Cell Metab, 2008. **8**(6): p. 512-21.
890 43. Listenberger, L., et al., *Decreasing Phosphatidylcholine on the Surface of the Lipid*
891 *Droplet Correlates with Altered Protein Binding and Steatosis.* Cells, 2018. **7**(12).
892 44. Titus, A.R., et al., *The C-Terminus of Perilipin 3 Shows Distinct Lipid Binding at*
893 *Phospholipid-Oil-Aqueous Interfaces.* Membranes (Basel), 2021. **11**(4).
894 45. Caillon, L., et al., *Triacylglycerols sequester monotopic membrane proteins to lipid*
895 *droplets.* Nat Commun, 2020. **11**(1): p. 3944.
896 46. Putta, P., et al., *Phosphatidic acid binding proteins display differential binding as a*
897 *function of membrane curvature stress and chemical properties.* Biochim Biophys Acta,
898 2016. **1858**(11): p. 2709-2716.
899 47. Chorlay, A., L. Foret, and A.R. Thiam, *Origin of gradients in lipid density and surface*
900 *tension between connected lipid droplet and bilayer.* Biophys J, 2021. **120**(24): p. 5491-
901 5503.
902 48. Garten, M., et al., *Methyl-branched lipids promote the membrane adsorption of alpha-*
903 *synuclein by enhancing shallow lipid-packing defects.* Phys Chem Chem Phys, 2015.
904 **17**(24): p. 15589-97.

905 49. Wolins, N.E., et al., *S3-12, Adipophilin, and TIP47 package lipid in adipocytes.* J Biol
906 Chem, 2005. **280**(19): p. 19146-55.
907 50. Englander, S.W. and N.R. Kallenbach, *Hydrogen exchange and structural dynamics of*
908 *proteins and nucleic acids.* Q Rev Biophys, 1983. **16**(4): p. 521-655.
909 51. Skinner, J.J., et al., *Protein hydrogen exchange: testing current models.* Protein Sci, 2012.
910 **21**(7): p. 987-95.
911 52. Balasubramaniam, D. and E.A. Komives, *Hydrogen-exchange mass spectrometry for the*
912 *study of intrinsic disorder in proteins.* Biochim Biophys Acta, 2013. **1834**(6): p. 1202-9.
913 53. Vadas, O., et al., *Using Hydrogen-Deuterium Exchange Mass Spectrometry to Examine*
914 *Protein-Membrane Interactions.* Methods Enzymol, 2017. **583**: p. 143-172.
915 54. Hickenbottom, S.J., et al., *Structure of a lipid droplet protein; the PAT family member*
916 *TIP47.* Structure, 2004. **12**(7): p. 1199-207.
917 55. Hynson, R.M., et al., *Solution structure studies of monomeric human TIP47/perilipin-3*
918 *reveal a highly extended conformation.* Proteins, 2012. **80**(8): p. 2046-55.
919 56. Weis, D.D., et al., *Identification and characterization of EX1 kinetics in H/D exchange*
920 *mass spectrometry by peak width analysis.* J Am Soc Mass Spectrom, 2006. **17**(11): p.
921 1498-1509.
922 57. Jumper, J., et al., *Highly accurate protein structure prediction with AlphaFold.* Nature,
923 2021. **596**(7873): p. 583-589.
924 58. Baek, M., et al., *Accurate prediction of protein structures and interactions using a three-*
925 *track neural network.* Science, 2021. **373**(6557): p. 871-876.
926 59. Najt, C.P., et al., *Structural and functional assessment of perilipin 2 lipid binding*
927 *domain(s).* Biochemistry, 2014. **53**(45): p. 7051-66.
928 60. Milov, A., K. Salikhov, and M. Shirov, *Application of ELDOR in electron-spin echo for*
929 *paramagnetic center space distribution in solids.* Fizika Tverdogo Tela, 1981. **23**(4): p.
930 975-982.
931 61. Pannier, M., et al., *Characterization of Ionic Clusters in Different Ionically Functionalized*
932 *Diblock Copolymers by CW EPR and Four-Pulse Double Electron−Electron Resonance.*
933 Macromolecules, 2001. **34**(16): p. 5555-5560.
934 62. Borbat, P.P. and J.H. Freed, *Pulse Dipolar Electron Spin Resonance: Distance*
935 *Measurements*, in *Structural Information from Spin-Labels and Intrinsic Paramagnetic*
936 *Centres in the Biosciences*, C.R. Timmel and J.R. Harmer, Editors. 2014. p. 1-82.
937 63. Borbat, P.P. and J.H. Freed, *Dipolar Spectroscopy - Single-resonance Methods.* Emagres,
938 2017. **6**(4): p. 465-493.
939 64. Borbat, P.P., E.R. Georgieva, and J.H. Freed, *Improved Sensitivity for Long-Distance*
940 *Measurements in Biomolecules: Five-Pulse Double Electron-Electron Resonance.* Journal
941 of Physical Chemistry Letters, 2013. **4**(1): p. 170-175.
942 65. Jeschke, G., *DEER Distance Measurements on Proteins*, in *Annual Review of Physical*
943 *Chemistry, Vol 63*, M.A. Johnson and T.J. Martinez, Editors. 2012. p. 419-446.
944 66. Bahrenberg, T., et al., *rDEER: A Modified DEER Sequence for Distance Measurements*
945 *Using Shaped Pulses.* Magnetochemistry, 2019. **5**(1).
946 67. Sung, Y.H. and D. Eliezer, *Residual structure, backbone dynamics, and interactions within*
947 *the synuclein family.* J Mol Biol, 2007. **372**(3): p. 689-707.

948 68. Tong, J.S., et al., *A scissors mechanism for stimulation of SNARE-mediated lipid mixing by*
949 *cholesterol.* Proceedings of the National Academy of Sciences of the United States of
950 America, 2009. **106**(13): p. 5141-5146.
951 69. Georgieva, E.R., et al., *Mechanism of influenza A M2 transmembrane domain assembly*
952 *in lipid membranes.* Sci Rep, 2015. **5**: p. 11757.
953 70. Borbat, P., et al., *Inter-helix distances in lysophospholipid micelle-bound alpha-synuclein*
954 *from pulsed ESR measurements.* Journal of the American Chemical Society, 2006.
955 **128**(31): p. 10004-10005.
956 71. Jeschke, G., et al., *Interresidual distance determination by four-pulse double electron-*
957 *electron resonance in an integral membrane protein: the Na+/proline transporter PutP*
958 *of Escherichia coli.* Biophysical Journal, 2004. **86**(4): p. 2551-2557.
959 72. Santinho, A., et al., *Membrane Curvature Catalyzes Lipid Droplet Assembly.* Curr Biol,
960 2020. **30**(13): p. 2481-2494 e6.
961 73. Ma, X., et al., *Validating an artificial organelle: Studies of lipid droplet-specific proteins*
962 *on adiposome platform.* iScience, 2021. **24**(8): p. 102834.
963 74. Skinner, J.R., et al., *Diacylglycerol enrichment of endoplasmic reticulum or lipid droplets*
964 *recruits perilipin 3/TIP47 during lipid storage and mobilization.* J Biol Chem, 2009.
965 **284**(45): p. 30941-8.
966 75. Joshi, A.S., et al., *Lipid droplet and peroxisome biogenesis occur at the same ER*
967 *subdomains.* Nat Commun, 2018. **9**(1): p. 2940.
968 76. King, C., et al., *ER membranes exhibit phase behavior at sites of organelle contact.* Proc
969 Natl Acad Sci U S A, 2020. **117**(13): p. 7225-7235.
970 77. Ajjaji, D., et al., *Hepatitis C virus core protein uses triacylglycerols to fold onto the*
971 *endoplasmic reticulum membrane.* Traffic, 2022. **23**(1): p. 63-80.
972 78. Khaddaj, R. and R. Schneiter, *Perilipin 3 promotes the formation of membrane domains*
973 *enriched in diacylglycerol and lipid droplet biogenesis proteins.* bioRxiv, 2022: p.
974 2022.09.14.507979.
975 79. Jacquier, N., et al., *Expression of oleosin and perilipins in yeast promotes formation of*
976 *lipid droplets from the endoplasmic reticulum.* J Cell Sci, 2013. **126**(Pt 22): p. 5198-209.
977 80. Zanghellini, J., F. Wodlei, and H.H. von Grunberg, *Phospholipid demixing and the birth of*
978 *a lipid droplet.* J Theor Biol, 2010. **264**(3): p. 952-61.
979 81. Kooijman, E.E., et al., *An electrostatic/hydrogen bond switch as the basis for the specific*
980 *interaction of phosphatidic acid with proteins.* J Biol Chem, 2007. **282**(15): p. 11356-64.
981 82. Mengistu, D.H., E.E. Kooijman, and S. May, *Ionization properties of mixed lipid*
982 *membranes: a Gouy-Chapman model of the electrostatic-hydrogen bond switch.* Biochim
983 Biophys Acta, 2011. **1808**(8): p. 1985-92.
984 83. Gimenez-Andres, M., et al., *Exceptional stability of a perilipin on lipid droplets depends*
985 *on its polar residues, suggesting multimeric assembly.* Elife, 2021. **10**.
986 84. Traikia, M., et al., *Formation of unilamellar vesicles by repetitive freeze-thaw cycles:*
987 *characterization by electron microscopy and 31P-nuclear magnetic resonance.* Eur
988 Biophys J, 2000. **29**(3): p. 184-95.
989 85. Dobbs, J.M., M.L. Jenkins, and J.E. Burke, *Escherichia coli and Sf9 Contaminant*
990 *Databases to Increase Efficiency of Tandem Mass Spectrometry Peptide Identification in*

Structural Mass Spectrometry Experiments. J Am Soc Mass Spectrom, 2020. **31**(10): p. 2202-2209.

86. Masson, G.R., et al., *Recommendations for performing, interpreting and reporting hydrogen deuterium exchange mass spectrometry (HDX-MS) experiments.* Nat Methods, 2019. **16**(7): p. 595-602.

87. Perez-Riverol, Y., et al., *The PRIDE database and related tools and resources in 2019: improving support for quantification data.* Nucleic Acids Res, 2019. **47**(D1): p. D442-D450.

88. Borbat, P.P., R.H. Crepeau, and J.H. Freed, *Multifrequency two-dimensional Fourier transform ESR: an X/Ku-band spectrometer.* J Magn Reson, 1997. **127**(2): p. 155-67.

89. Jeschke, G. and Y. Polyhach, *Distance measurements on spin-labelled biomacromolecules by pulsed electron paramagnetic resonance.* Physical Chemistry Chemical Physics, 2007. **9**(16): p. 1895-1910.

90. Gamliel, D. and J.H. Freed, *THEORY OF 2-DIMENSIONAL ESR WITH NUCLEAR MODULATION.* Journal of Magnetic Resonance, 1990. **89**(1): p. 60-93.

91. Tang, S.G., et al., *Structural basis for activation, assembly and membrane binding of ESCRT-III Snf7 filaments.* Elife, 2015. **4**.

92. Chiang, Y.W., P.P. Borbat, and J.H. Freed, *The determination of pair distance distributions by pulsed ESR using Tikhonov regularization.* Journal of Magnetic Resonance, 2005. **172**(2): p. 279-295.

93. Chiang, Y.W., P.P. Borbat, and J.H. Freed, *Maximum entropy: a complement to Tikhonov regularization for determination of pair distance distributions by pulsed ESR.* Journal of magnetic resonance (San Diego, Calif.: 1997), 2005a. **177**(2): p. 184-196.

94. Borbat, P.P. and J.H. Freed, *Measuring distances by pulsed dipolar ESR spectroscopy: spin-labeled histidine kinases.* Methods Enzymol, 2007. **423**: p. 52-116.

95. Bode, B.E., et al., *Counting the monomers in nanometer-sized oligomers by pulsed electron - Electron double resonance.* Journal of the American Chemical Society, 2007. **129**(21): p. 6736-6745.

96. Milov, A.D., A.B. Ponomarev, and Y.D. Tsvetkov, *Modulation beats of signal of double electron-electron resonance in spin echo for biradical systems* Journal of Structural Chemistry, 1984. **25**(5): p. 710-713.

97. Thiam, A.R., et al., *COPI buds 60-nm lipid droplets from reconstituted water-phospholipid-triacylglyceride interfaces, suggesting a tension clamp function.* Proc Natl Acad Sci U S A, 2013. **110**(33): p. 13244-9.

98. Chorlay, A., A. Santinho, and A.R. Thiam, *Making Droplet-Embedded Vesicles to Model Cellular Lipid Droplets.* STAR Protoc, 2020. **1**(3): p. 100116.

99. Oeffner, R.D., et al., *Putting AlphaFold models to work with phenix.process_predicted_model and ISOLDE.* Acta Crystallogr D Struct Biol, 2022. **78**(Pt 11): p. 1303-1314.

100. Kokorin, A.I., *Nitroxides - Theory, Experiment and Applications*. 2012, Rijeka: IntechOpen. 448.

101. Rabenstein, M.D. and Y.K. Shin, *Determination of the distance between two spin labels attached to a macromolecule.* Proc Natl Acad Sci U S A, 1995. **92**(18): p. 8239-43.

1035
1036

Acknowledgements

This work was supported by in part by the NIGMS (R35GM128666, MVA), the Sloan Research Foundation (MVA), the Natural Science and Engineering Research Council of Canada (Discovery Grant 2020-04241, JEB) with salary support from the Michael Smith Foundation for Health Research (Scholar award 17868, JEB), the ANR (18-CE11-0012-01-MOBIL, CE11-0032-02-LIPRODYN and 21-CE13-0014-LIPDROPER, ART), and the NSF (CBET 1903189 and DGE 1922639, SRB). ESR study, conducted at ACERT, was supported by NIH/NIGMS grants 1R24GM146107 and P41GM103521.

Author contributions

YMC generated constructs for E. coli and mammalian cell expression, purified all proteins, conducted liposome sedimentation, artificial lipid droplet binding assays, CD, DLS with assistance from SF, prepared figures, and wrote the initial draft. DA conducted all DEV and cell culture experiments. KDF, MLJ, and BEM setup, analyzed, and/or prepared figures and text from the HDX-MS data. PPB designed, acquired, analyzed, and prepared figures for all PDS-ESR data. JEB, ART, JHF, SRB and MVA supervised the work and provided funding support.

Competing Interest Statement

JEB reports personal fees from Scorpion Therapeutics and Olema Oncology; and research grants from Novartis.

1068 **Figures and Figure Legends**

1069

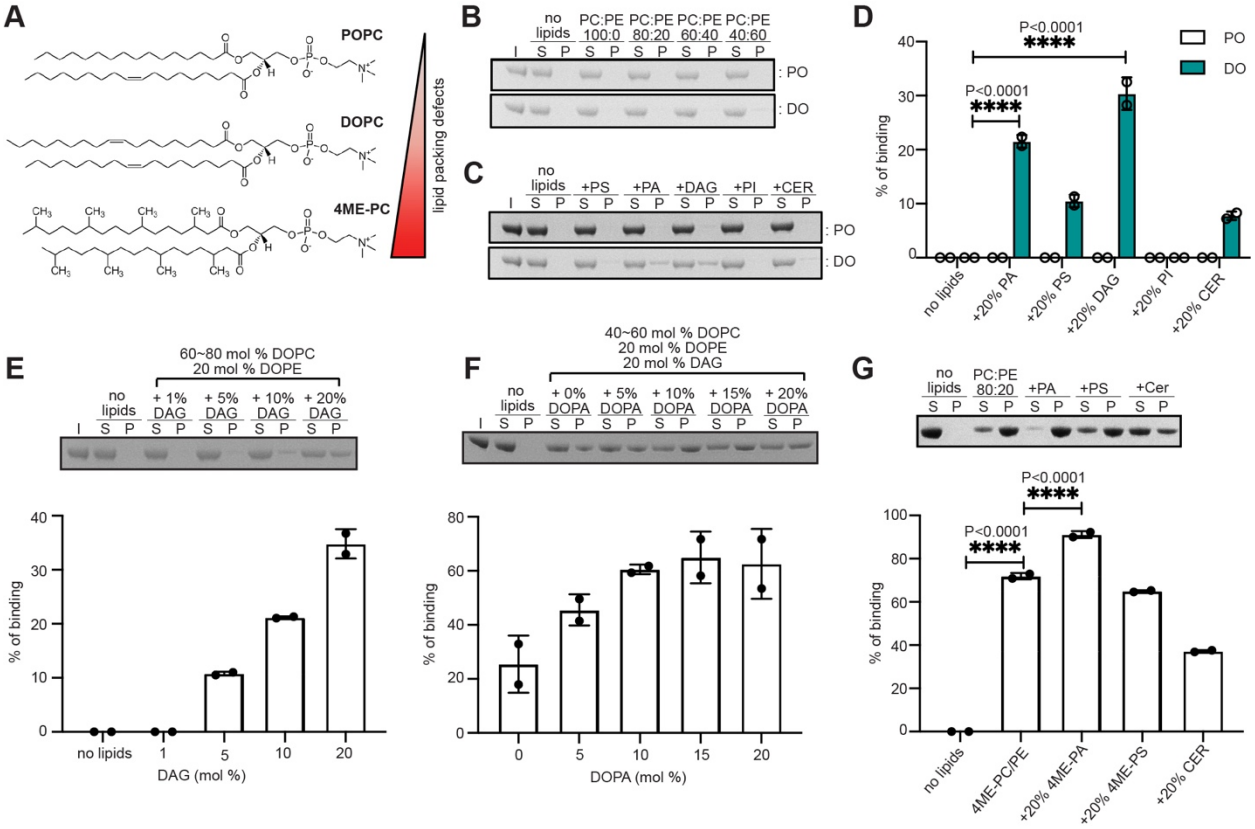

1070

1071 **Figure 1. Triglyceride precursors DAG and PA recruit PLIN3 to membrane bilayers**

1072 **A)** Structures of representative phospholipids used in this study.

1073 **B)** SDS-PAGE analysis of human PLIN3 liposome sedimentation assay on the either palmitoyl-
1074 oleoyl (PO)-liposomes or di-oleoyl (DO)-liposomes in different ratio of PC to PE. Lane S
1075 (supernatant) and P (pellet) represent unbound and bound human PLIN3 to liposomes.

1076 **C)** SDS-PAGE analysis of human PLIN3 recruitment to liposomes enriched with 20 mol% of the
1077 additional lipids PS, PA, DAG, PI and ceramide.

1078 **D)** Quantification of PLIN3 recruitment to liposomes in different lipid compositions (n=2).
1079 Statistical analysis was performed using two-way ANOVA (****, $p<0.0001$).

1080 **E)** SDS-PAGE analysis of human PLIN3 recruitment to DO-liposomes using different amounts
1081 of DAG. DOPE concentration was held constant at 20mol% and DOPC was adjusted between
1082 60 and 80mol% to maintain total phospholipid concentration. Bar graph shows addition of DAG
1083 increases PLIN3 binding.

1084 **F)** SDS-PAGE analysis of human PLIN3 recruitment to DO-liposomes enriched with different
1085 amount of DOPA. The amounts of DOPE and DAG were kept constant at 20mol%. DOPC
1086 concentration was adjusted between 40 and 60mol% to maintain total phospholipid
1087 concentration. Bar graph shows addition of DOPA further increases PLIN3 binding.

1088 **G)** SDS-PAGE analysis of human PLIN3 recruitment to 4ME liposomes enriched with 20 mol%
1089 of the additional lipids 4ME-PA, 4ME-PS, ceramide. 4ME-PC and 4ME-PE concentrations
1090 ranged between 60 ~80mol% and 20mol%, respectively. Statistical analysis for quantification of
1091 liposome binding was performed using ordinary one-way ANOVA with Tukey's multiple
1092 comparison test (n=2, ****,$p<0.0001$)

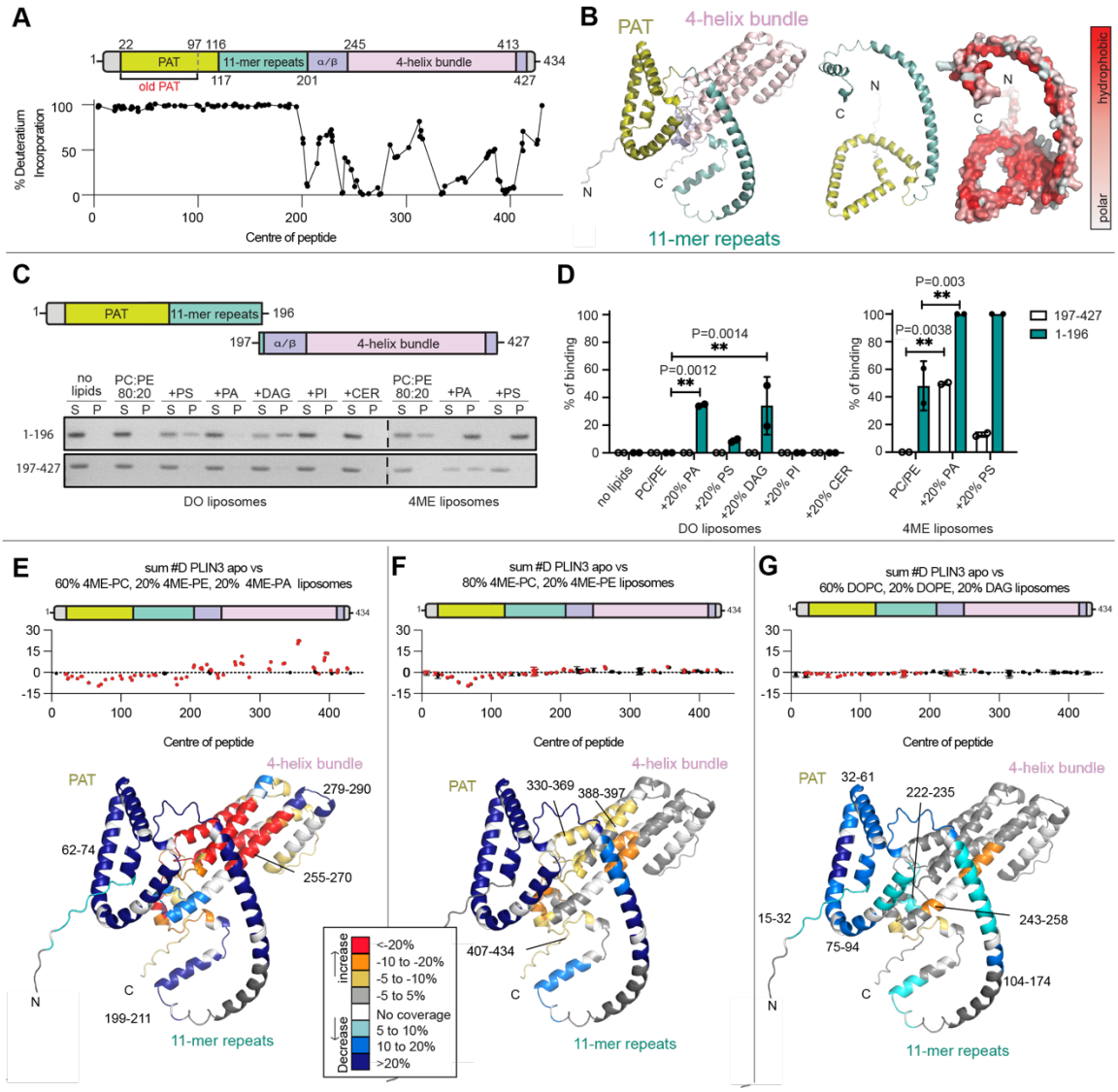

Figure 2. HDX-MS analysis of PLIN3 membrane binding

A) Absolute percentage of deuterium incorporation after 3sec deuterium exposure of PLIN3 at 1°C in the absence of liposomes. Each point represents a single peptide, with them being graphed on the x-axis according to their central residue. A domain architecture of human PLIN3 was drawn to match the scale of x-axis of HDX-MS. N-terminal PAT domain (mustard) and 11-mer repeats (cyan) have no detectable secondary structure in the absence of liposomes.
B) A predicted 3D structure of human PLIN3 (UniProt: O60664) by AlphaFold (Left). The surface of PAT domain and 11-mer repeats were shown according to the hydrophobicity (Right).
C) SDS-PAGE and **D)** quantitative analysis of PAT/11-mer repeats and 4-helix bundle liposome binding. DO and 4ME-liposomes were prepared in the same way as Figure 1C and 1D. Statistical analysis for quantification of liposome binding was performed using two-way ANOVA with Tukey's multiple comparison test (n=2).
E-G) Quantitative analysis of deuterium exchange differences of human PLIN3 in the presence of liposomes. The sum of the difference in the # of incorporated deuterons is shown for the absence and the presence of liposomes over all timepoints. The N-terminus composed of

PAT/11-mer repeats was significantly protected from deuterium exchange (defined as > 5% change in exchange, > 0.4 Da mass difference in exchange, a *p*-value < 0.01 using a two-tailed Student's *t*-test). Each point represents an individual peptide, with those colored in red having a significant difference, with error bars showing standard deviation (n=3). Liposomes were generated with **(E)** 60mol% 4ME-PC, 20mol% 4ME-PE and 20mol% 4ME-PA, **(F)** 80mol% 4ME-PC, 20mol% 4ME-PE or **(G)** 60mol% DOPC, 20mol% DOPE and 20mol% DAG. A map of deuterium exchange rate according to all peptides throughout the entire PLIN3 was generated based on the AlphaFold predicted PLIN3 structure and color coded according to the legend. The full set of peptides is shown in the source data.

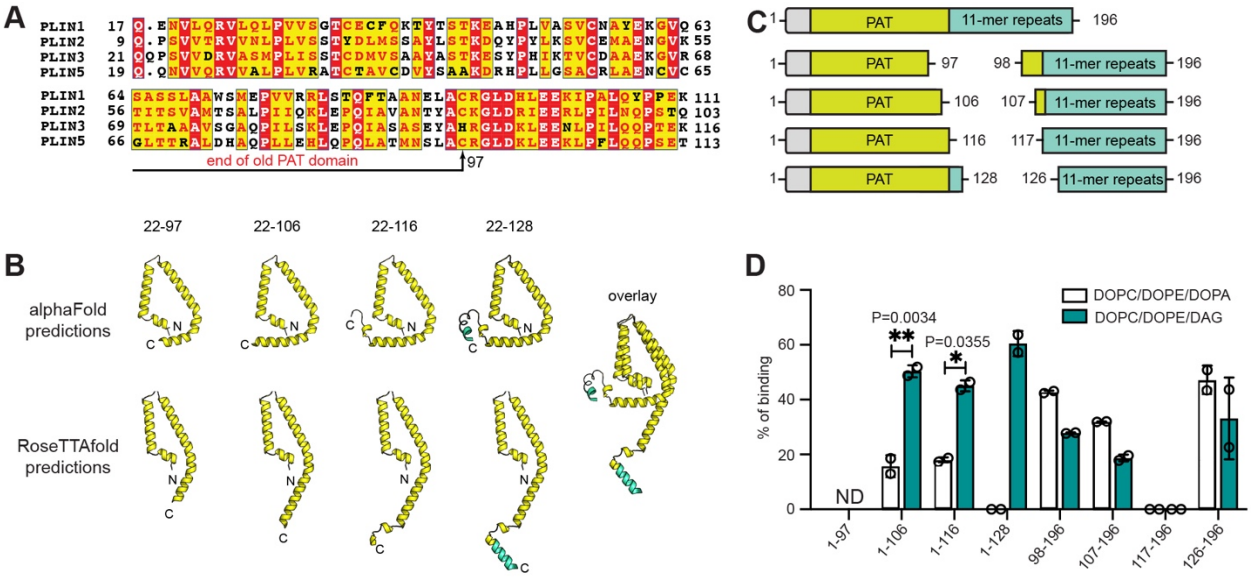

Figure 3. An expanded PAT domain binds DAG enriched membranes

A) Multiple sequence alignment of the N-terminus of human PLIN 1 (UniProt: O60240), PLIN2 UniProt: Q99541), PLIN3 (UniProt: O60664), and PLIN5 (UniProt: Q00G26). The previously suggested PAT domain (residues 1-97) is indicated with black arrow.

B) Putative PAT domain triangular structures predicted by both AlphaFold and RoseTTAFold.

C) Schematic of PAT domain constructs and the counterpart 11-mer repeats constructs.

D) Quantitative analysis of liposome recruitment for various PAT domain and 11-mer repeats constructs. Statistical analysis for quantification of liposome binding was performed using two-way ANOVA with Tukey's multiple comparison test (n=2).

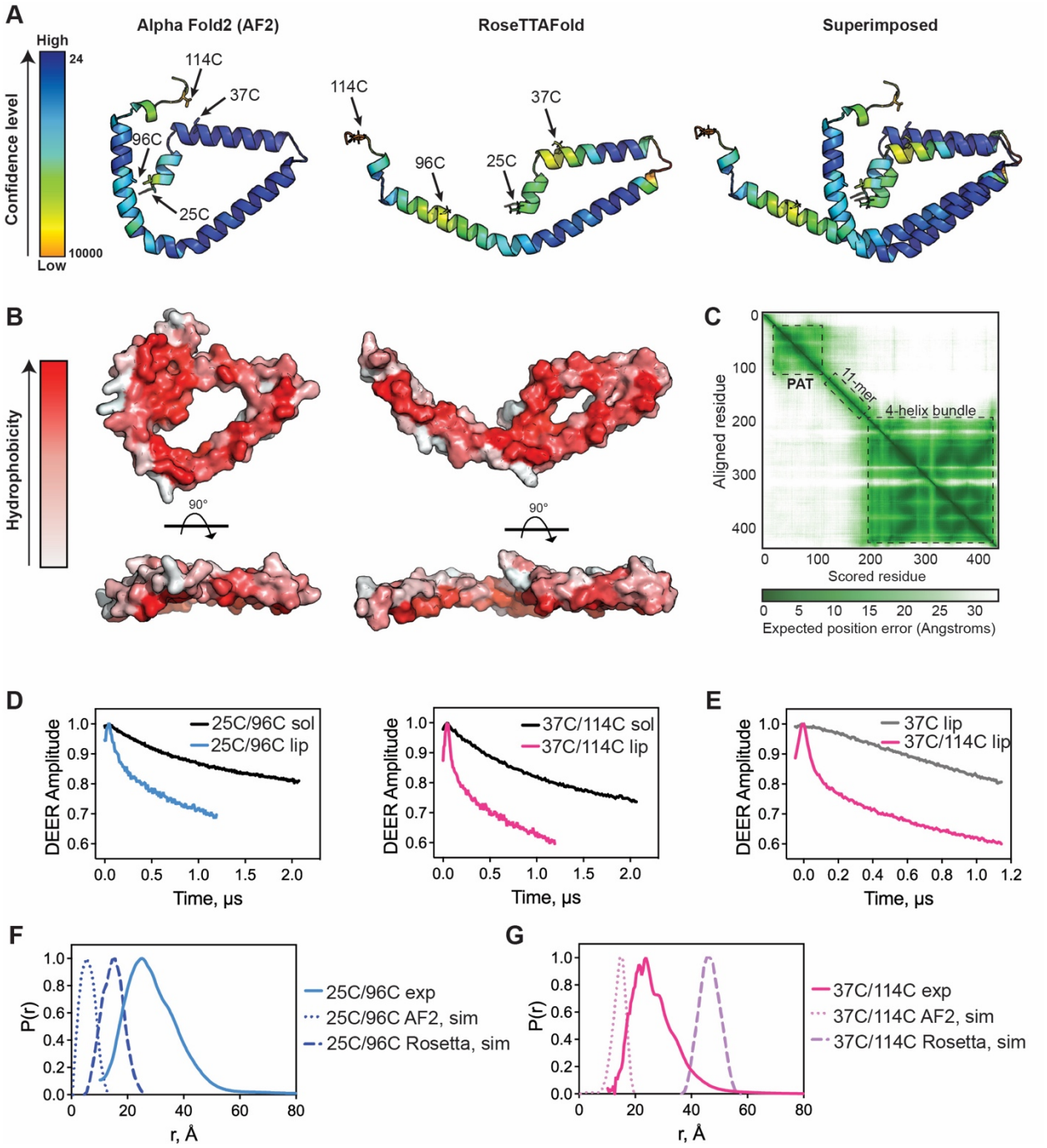

Figure 4. Membrane-induced conformational rearrangements are consistent with a PAT domain tertiary structure

A) Cartoon representation of the PAT domain structure predicted by AlphaFold2 and RoseTTAFold with relative confidence levels shown. The positions of the spin-labeled residues are indicated with arrows.

B) The hydrophobic surface of predicted PAT domain are depicted. The hydrophobic face of the helices is facing towards the reader.

C) The PAE (Predicted Aligned Error) value of AlphaFold2 for full length PLIN3 was plotted by ChimeraX and shown as an interactive 2D plot (bottom, right panel).

D) Time domain signals from DEER spectroscopy of double-labeled 25C/96C (left) and 37C/114C (right) in solution (sol) and on liposomes (lip).
E) Time domain signals from DEER spectroscopy of double-labeled 37C/114C and single-labeled 37C proteins on liposomes.
F, G) Distance distributions from DEER spectroscopy of **(E)** 25C/96C and **(F)** 37C/114C determined experimentally (exp) and from MtsslWizard simulations using the AlphaFold2 (AF2, sim) and RoseTTAFold (Rosetta, sim) predicted structures.

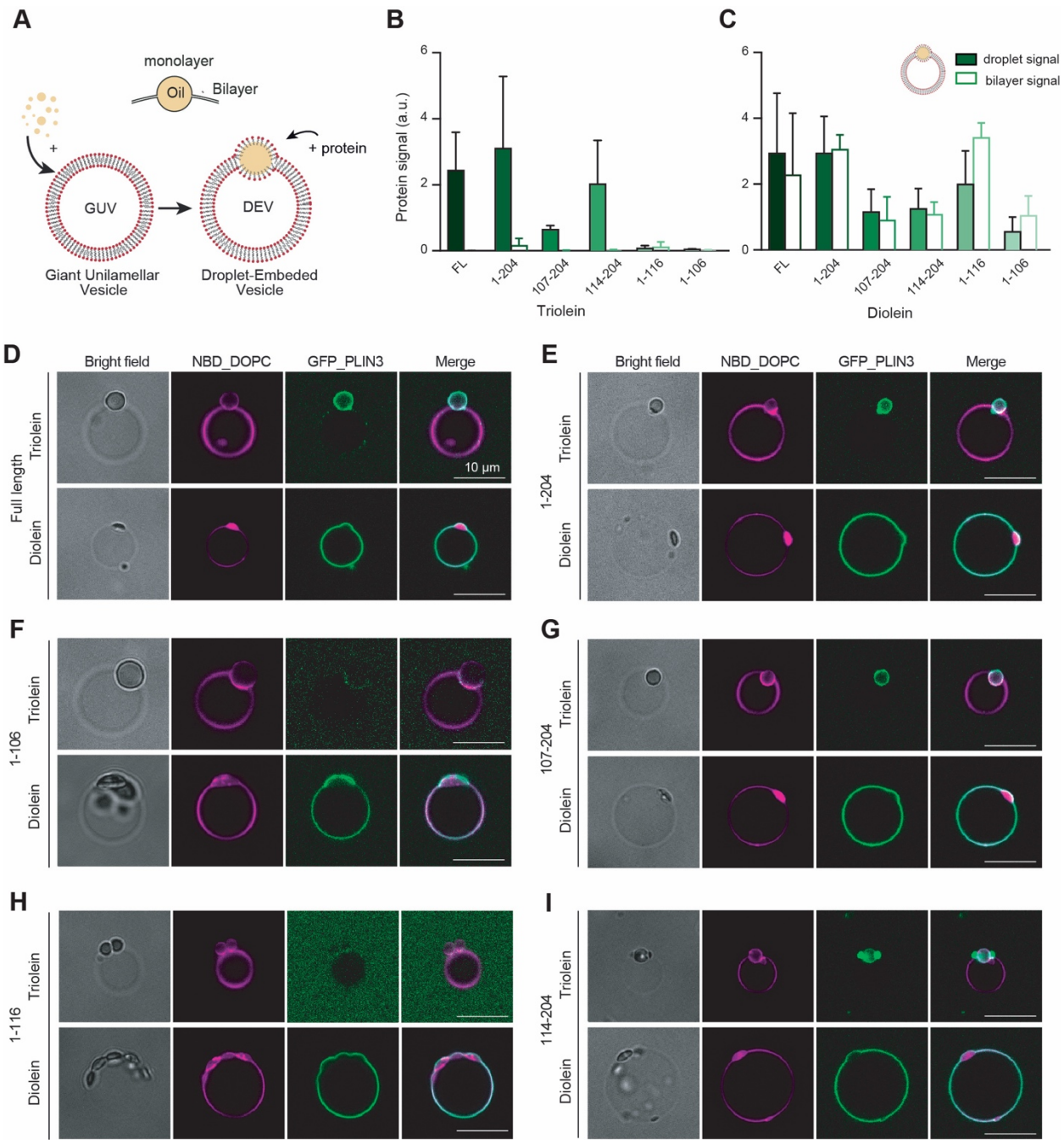

Figure 5. **DAG recruits PLIN3 to membrane bilayers and LD droplets in vitro**

A) A diagram of generation of DEVs by mixing oils and giant unilamellar vesicles (GUVs).

B, C) Quantification of the recruitment of GFP tagged PLIN3 constructs to droplet embedded vesicles (DEVs) containing (B) triolein or (C) Diolein**.** Statistical analysis was done with a Mann–Whitney non-parametric test. $P<0.01$ for all proteins. Three different experiments were performed and 10 to 15 DEVs quantified for each experiment.

D-I) Fluorescent microscopic images of N-terminal GFP tagged full length and PLIN3 constructs (green) comprised of PAT domain and 11-mer repeats to (DEVs) (magenta) that are generated with fluorescent labeled phospholipids and oils. F) and H) Recruitment of PAT domain constructs. Almost no recruitment of PAT domain constructs in the presence of Triolein. G) and I) Recruitment of 11-mer repeats constructs.

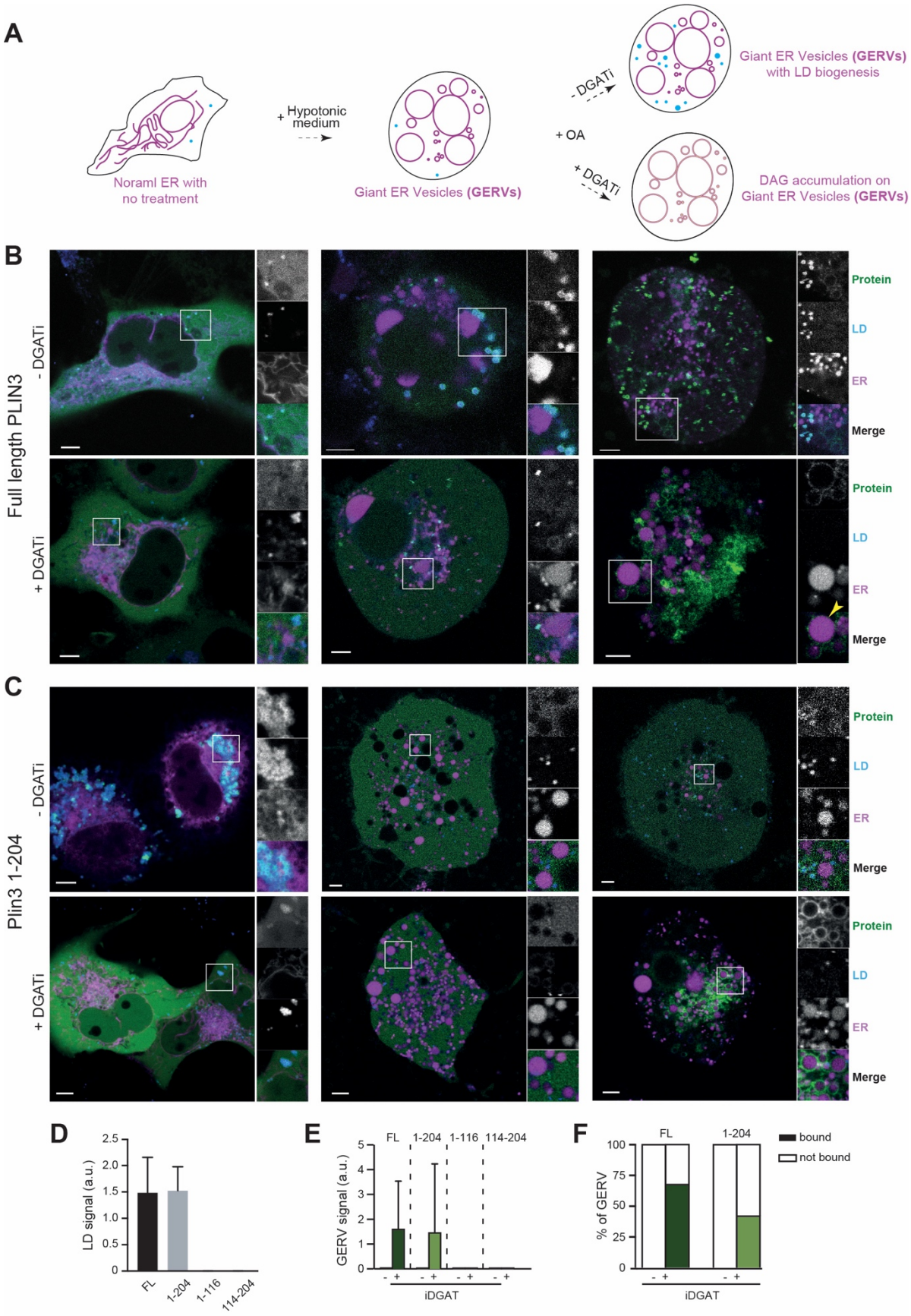
A
Noraml ER with no treatment
+ Hypotonic medium
Giant ER Vesicles (GERVs)
- DGATi
Giant ER Vesicles (GERVs) with LD biogenesis
+ OA
+ DGATi
DAG accumulation on Giant ER Vesicles (GERVs)
B
Full length PLIN3
- DGATi
+ DGATi
Protein
LD
ER
Merge
C
Plin3 1-204
D
LD signal (a.u.)
FL
1-204
1-116
114-204
E
GERV signal (a.u.)
iDGAT
F
% of GERV
bound
not bound

1229

Figure 6. Both PAT domain and 11-mer repeats are necessary for PLIN3 recruitment to DAG enriched ER membranes in Cos7 cells

A) A diagram of treatment of Giant ER Vesicle formation and treatment of oleic acid and DGATi to induce DAG accumulation on the ER in Cos7 cells.

B, C) Subcellular localization of GFP tagged full length PLIN3 and PAT/11-mer repeats (1-204) were visualized in green in Cos7 cells under fluorescent microscope ZEISS LSM800 Airyscan. ER was visualized with ER specific marker RFP-KDEL in magenta. Lipid droplets were labeled with LipidTox Deepred to stain neutral lipids in cyan. After treated with hypotonic medium, cells were supplemented with oleate in the presence or absence of DGAT1/2 inhibitors. Each experiment was performed more than 3 times.

D) Quantification of the amount of various PLIN3 constructs on LDs

E) Quantification of the amount of various PLIN3 constructs on GERV after oleate treatment in the presence and the absence of DGAT1/2 inhibitors.

F) % of GERV that are covered with full length PLIN3 or PAT/11-mer repeats construct (1-204) after oleate treatment in the presence and the absence of DGAT1/2 inhibitors.

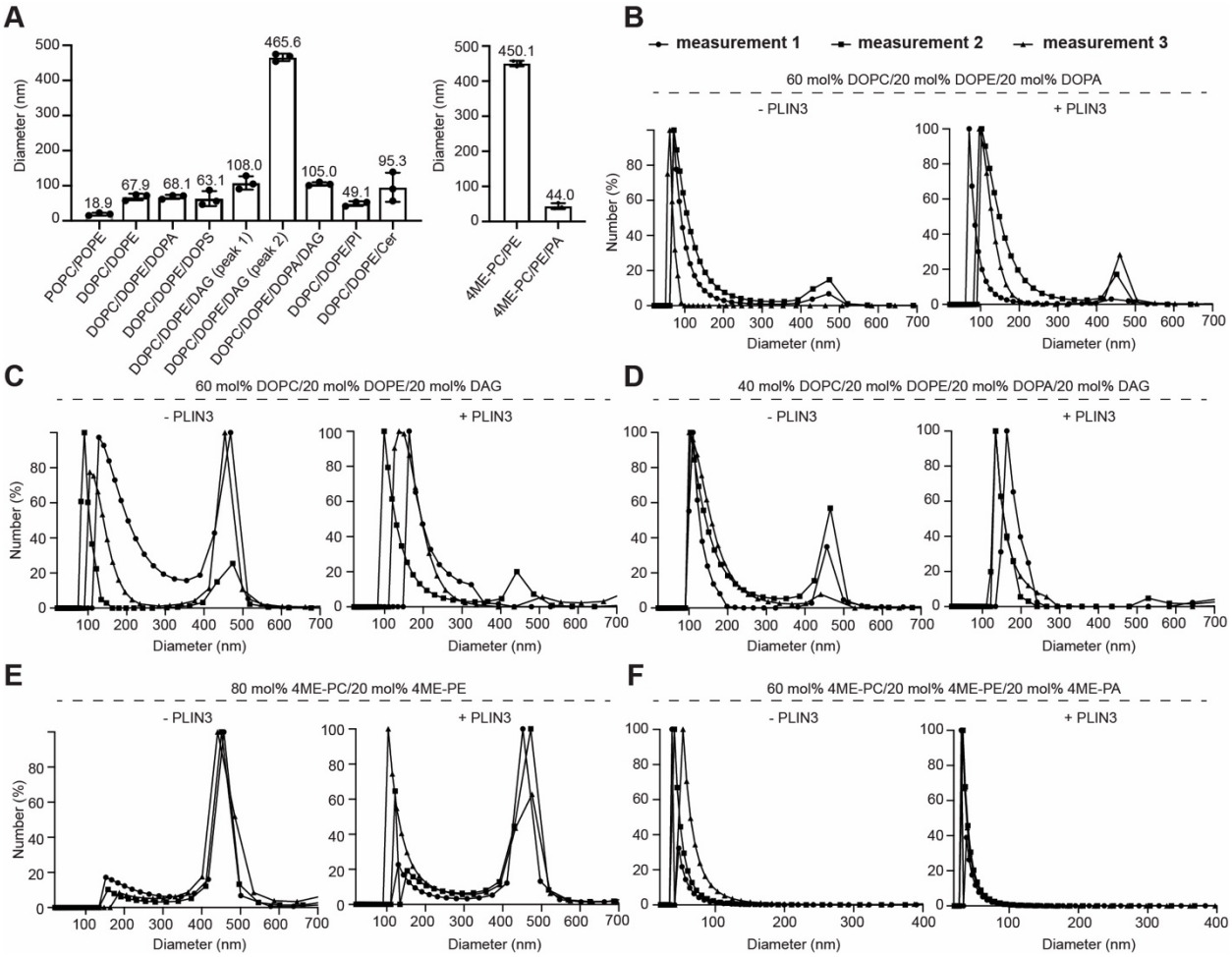

Supplementary Figure 1.

A) DLS analysis of liposomes with different lipid composition. For each liposome, three measurements were plotted.

B-F) DLS analysis of different liposomes with or without full length PLIN3. For each liposome, the number average size distribution (%) was recorded and plotted (n=3) in the presence and absence of full length PLIN3.

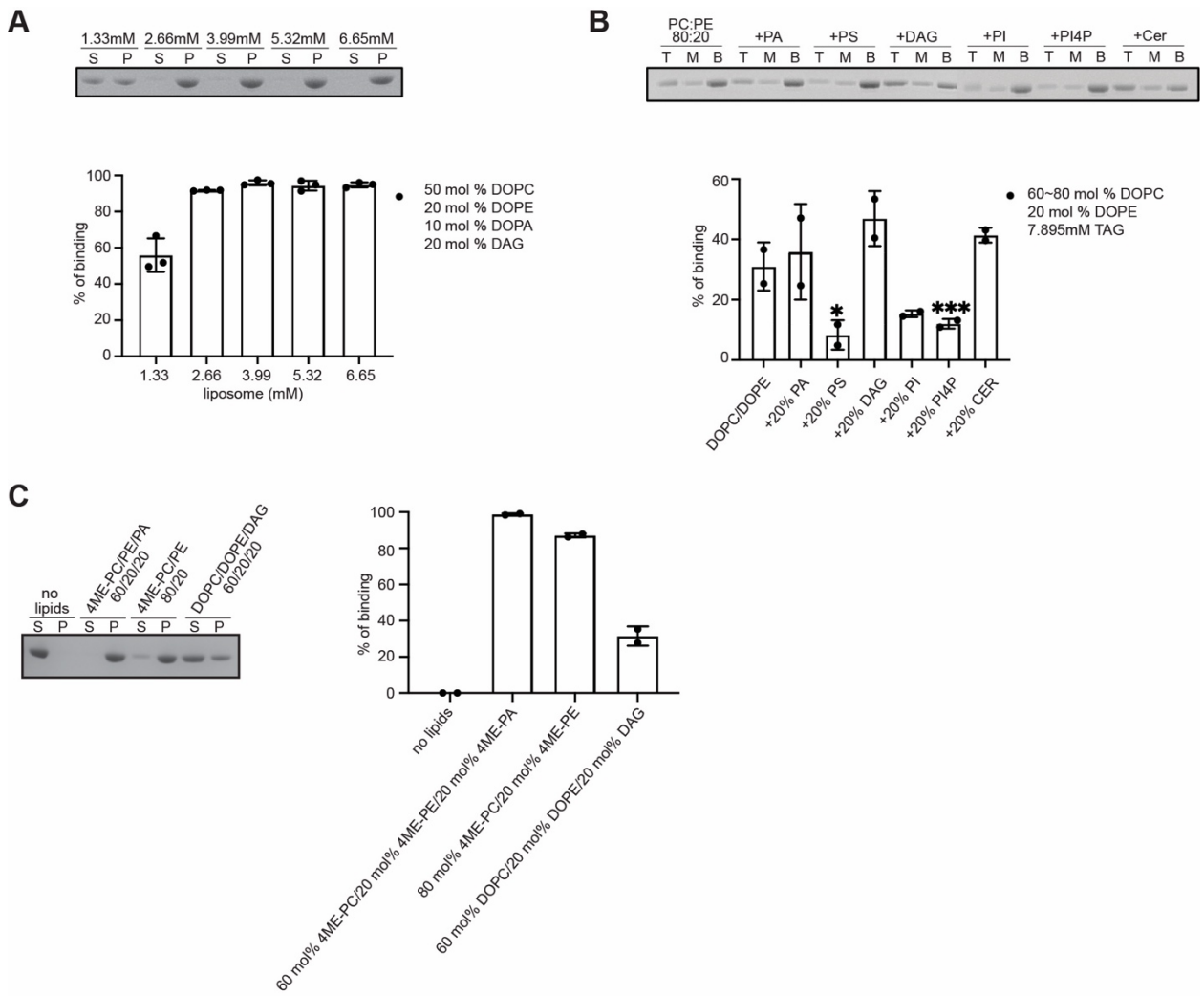

Supplementary Figure 2.

A) SDS-PAGE and quantitative analysis of human PLIN3 recruitment by increasing the total amount of liposomes. The molar ratio of DOPC/DOPE/DOPA/DAG in 50:20:10:20 was kept same. Lane S represents unbound human PLIN3 from supernatant. Lane P represents pelleted human PLIN3 that bound to liposomes. Bar graph shows total increase in liposome amount results almost 100% recruitment of PLIN3 to liposome.

B) SDS-PAGE and quantitative analysis of human PLIN3 recruitment to ALDs generated with DO-phospholipids and TAGs (C16) by adding additional with 20 mol% of lipids such as PS, PA, DAG, PI, PI4P and ceramide. Top, middle and bottom fractions after sucrose-gradient centrifuge were indicated as T, M and B, respectively. Statistical analysis was performed using ordinary one-way ANOVA with Tukey's multiple comparison test (n=2, *, p=0.0258, ***,p=0.004).

C) SDS-PAGE and quantitative analysis of human PLIN3 recruitment to liposomes in buffer containing 100mM NaCl and 20mM HEPES pH 7.0. Three different liposomes that were applied in HDX-MS were generated. Lane S represents unbound human PLIN3 from supernatant. Lane P represents pelleted human PLIN3 that bound to liposomes.

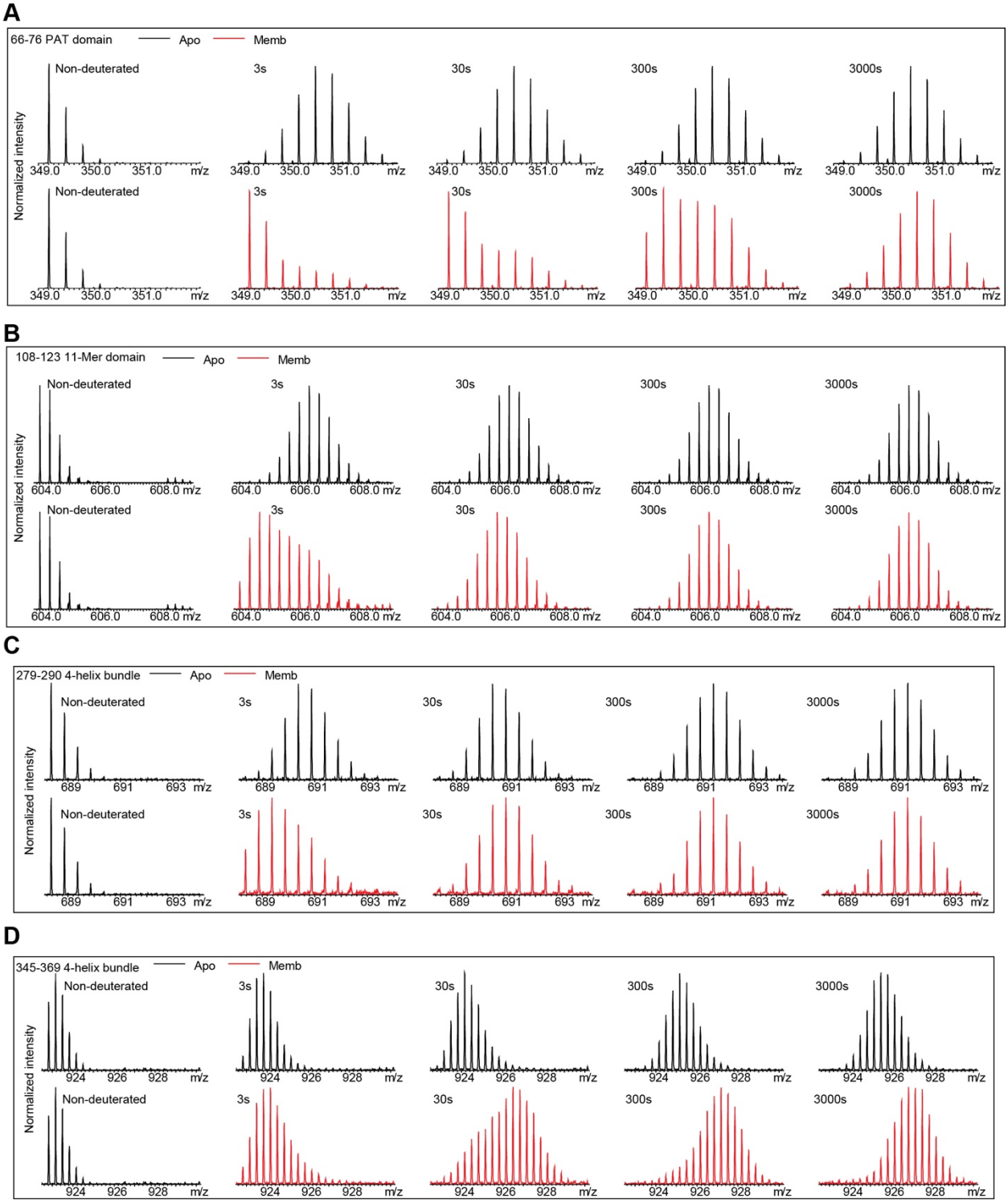

Supplementary Figure 3.
Representative bimodal distribution mass spectra from the peptides at PAT domain, 11-mer repeats, and 4-helix bundle of PLIN3 after deuterium exchange.

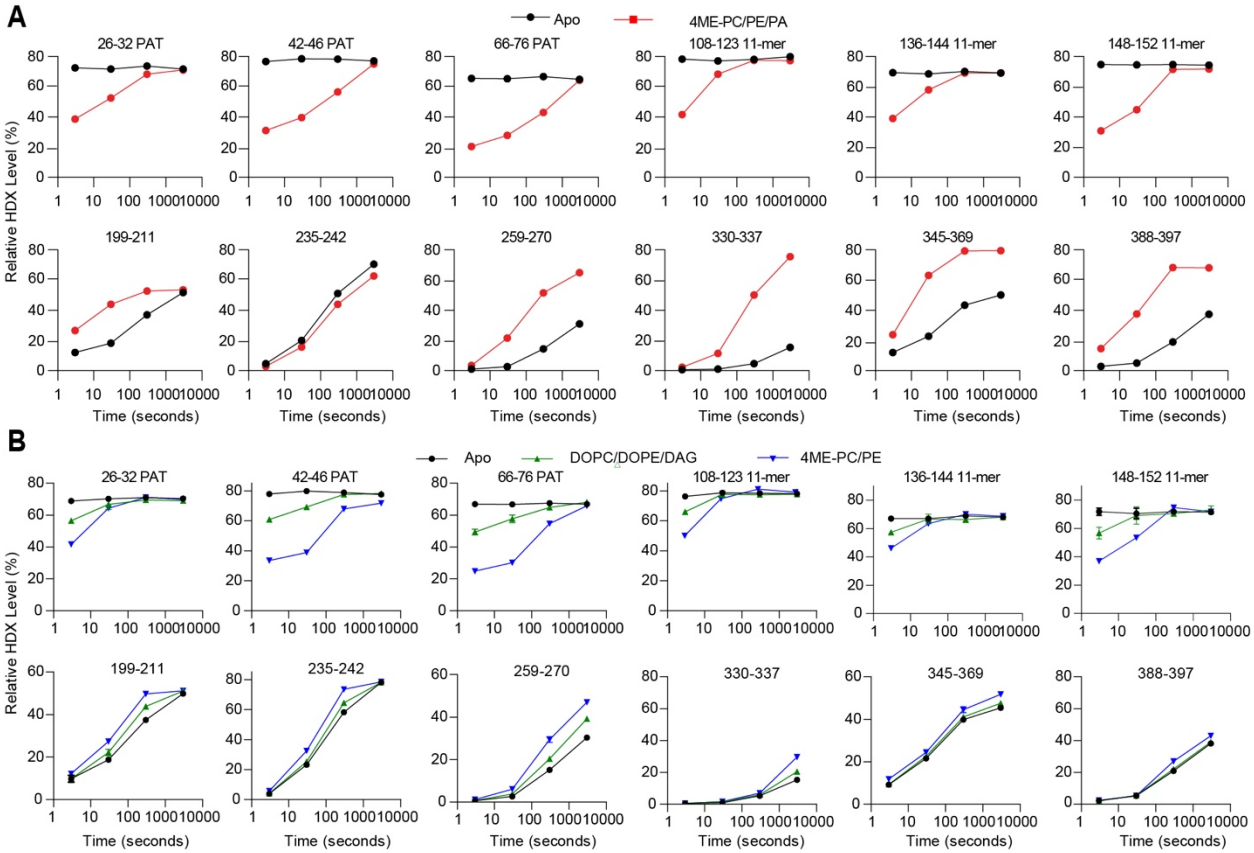

Supplementary Figure 4.

A) Deuterium exchange uptake plots for selected peptides in the PAT domain, 11-mer repeats and 4-helix bundle were plotted across all timepoints as 3s, 30s, 300s and 3000s. Data points in the absence and presence of liposomes were colored in black and red, respectively. Liposomes were generated with 60 mol% 4ME-PC, 20 mol% 4ME-PE and 20 mol% 4ME-PA). All peptides are shown in the source data.

B) Deuterium exchange uptake plots for selected peptides in the presence of two different liposomes are plotted across all timepoints as 3s, 30s, 300s and 3000s colored according the the legend. All peptides are shown in the source data.

1341

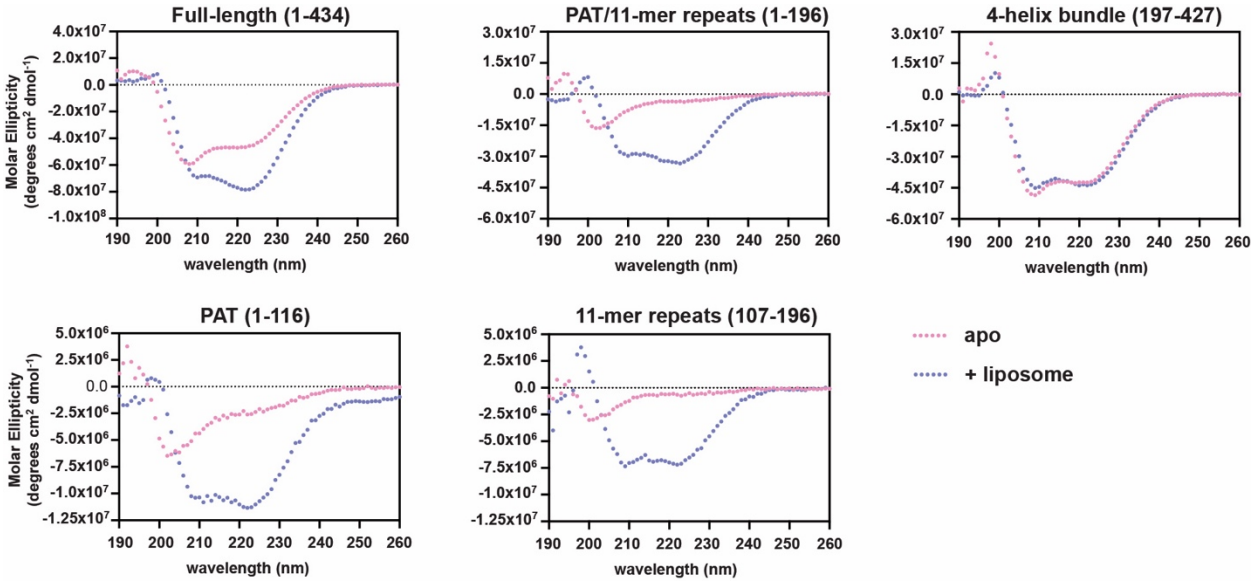

1342
1343
1344 **Supplementary Figure 5.** CD analysis of PLIN3 full length and various fragments with or
1345 without 4ME-PC/PE/PA liposomes
1346
1347
1348
1349
1350

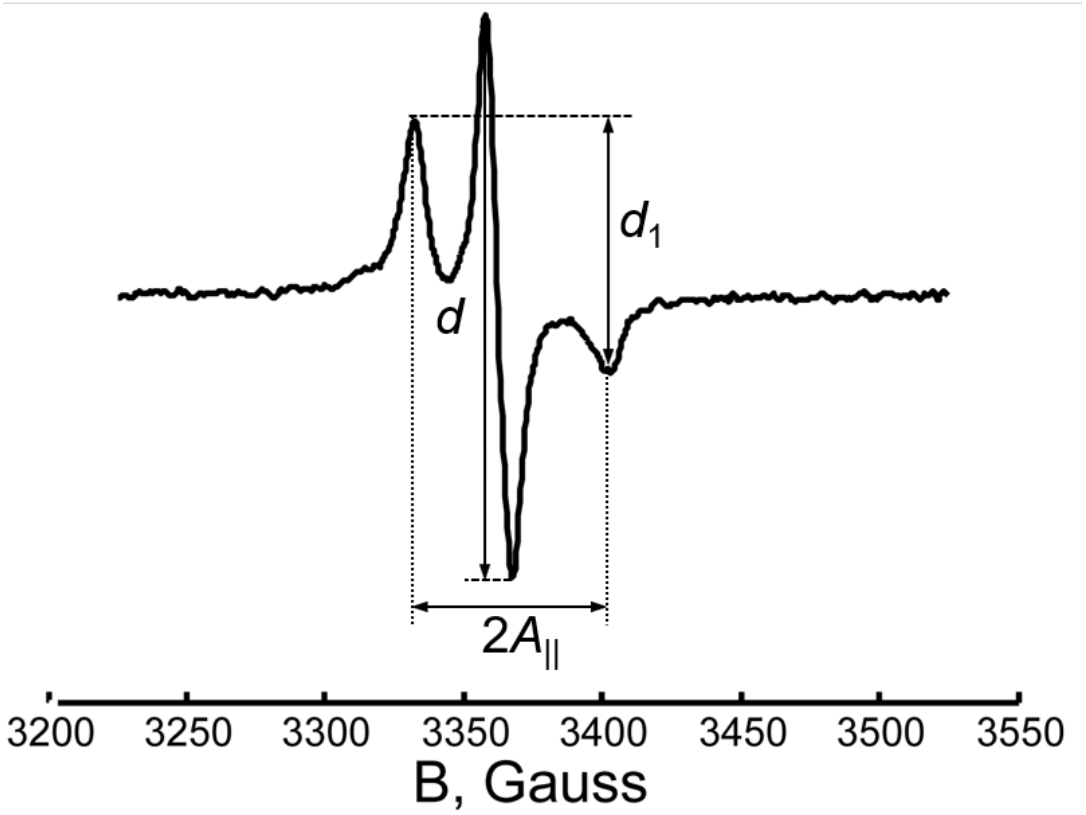

Supplementary Figure 6. CW ESR spectrum of 37C/144C in lipid recorded at 9,434 GHz frequency. The Parameter Δ, defined [100] as the ratio of d1/d, is 0.45, which for the MTSL spin label indicates the distance in range of 1.5-2.0 nm [100, 101], i.e. somewhat shorter than reported by DEER which has reduced sensitivity to distances below 2.0 nm.

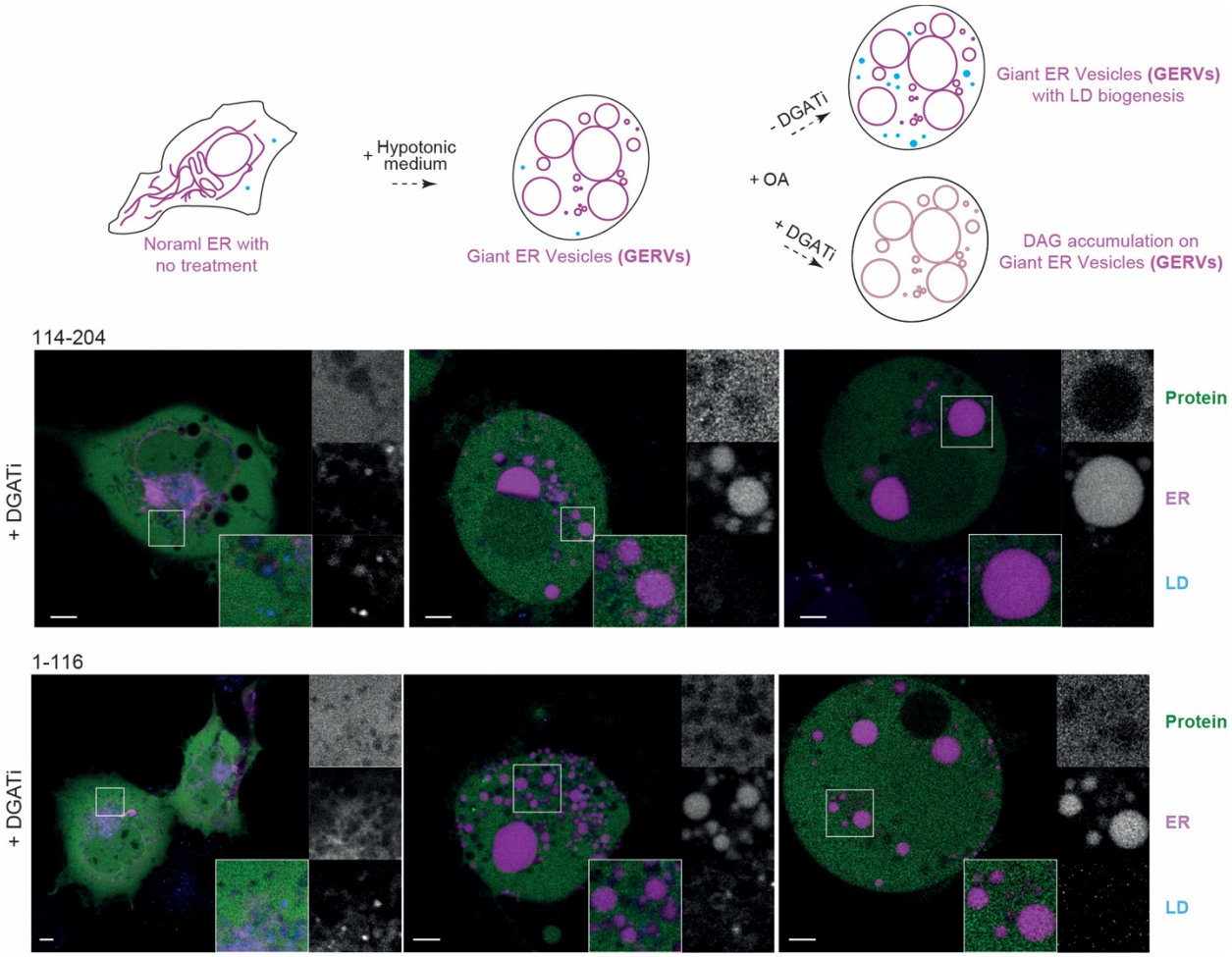

Supplementary Figure 7.
Subcellular localization of GFP tagged 114-204 and 1-116 constructs of PLIN3 was visualized in green in Cos7 cells under fluorescent microscope ZEISS LSM800 Airyscan. ER was visualized with ER specific marker RFP-KDEL in magenta. Lipid droplets were labeled with LipidTox Deepred to stain neutral lipids in cyan. After treated with hypotonic medium, cells were supplemented with oleate in the presence or absence of DGAT1/2 inhibitors.

1398 **Supplementary Table 1**.
1399 Summary of all HDX-MS data processing.

Data set	PLIN3 order disorder Expt-1	PLIN3 Apo Expt-2	PLIN3 + 60% 4ME-PC, 20% 4ME-PE, 20% 4ME-PA liposomes Expt-2	PLIN3 Apo Expt-3	PLIN3 + 60% DOPC, 20% DOPE, 20% DAG liposomes Expt-3	PLIN3+ + 80% 4ME-PC, 20% 4ME-PE liposomes Expt-3
HDX reaction details	%D2O=84.9 % pH(read)=7.5 Temp=20ºC	%D2O=63% pH(read)=8.0 Temp=20ºC	%D2O=63% pH(read)=8.0 Temp=20ºC	%D2O=72% pH(read)=8.0 Temp=20ºC	%D2O=72% pH(read)=8.0 Temp=20ºC	%D2O=72% pH(read)=8.0 Temp=20ºC
HDX time course (seconds)	0.3s, fully deuterated	3s, 30s, 300s, 3000s	3s, 30s, 300s, 3000s	3s, 30s, 300s, 3000s	3s, 30s, 300s, 3000s	3s, 30s, 300s, 3000s
HDX controls	FD	N/A	N/A	N/A	N/A	N/A
Back-exchange	Corrected by fully deuterated sample	No correction, deuterium levels are relative	No correction, deuterium levels are relative	No correction, deuterium levels are relative	No correction, deuterium levels are relative	No correction, deuterium levels are relative
Number of peptides	144	90	90	90	90	90
Sequence coverage	99.8%	91.7%	91.7%	91.7%	91.7%	91.7%
Average peptide /redundancy	Length= 17.3 Redundancy = 5.4	Length= 13.0 Redundancy = 2.6	Length= 13.0 Redundancy = 2.6	Length= 13.0 Redundancy = 2.6	Length= 13.0 Redundancy = 2.6	Length= 13.0 Redundancy= 2.6
Replicates	3	3	3	3	3	3
Repeatability	Average StDev=0.4%	Average StDev=0.6%	Average StDev=0.6%	Average StDev=0.8%	Average StDev=1.0%	Average StDev=0.9%
Significant differences in HDX	N/A	>5% and >0.4 Da and unpaired t-test ≤0.01	>5% and >0.4 Da and unpaired t-test ≤0.01	>5% and >0.4 Da and unpaired t-test ≤0.01	>5% and >0.4 Da and unpaired t-test ≤0.01	>5% and >0.4 Da and unpaired t-test ≤0.01

1400
1401
1402
1403
1404
1405
1406
1407

Supplementary Information 1

Codon optimized DNA sequence of human perilipin 3

```
ATGTCTGCTGATGGTGCTGAAGCTGACGGTAGCACCCAGGTAACCGTTGAAGAACCGGTTCAGCAGCCGTCTGTTGTT
GACCGTGTAGCTTCTATGCCGCTGATCTCTAGCACCTGCGATATGGTGAGCGCGGCGTACGCGTCTACTAAAGAATCT
TACCCGCACATCAAAACCGTTTGCGACGCTGCTGAAAAAGGTGTTCGTACCCTGACCGCTGCTGCTGTTTCTGGTGCG
CAGCCGATCCTGAGCAAGCTGGAACCGCAGATCGCGTCTGCTTCTGAATACGCGCACCGCGGTCTGGACAAACTGGAA
GAAAACCTGCCGATTCTGCAGCAGCCGACCGAAAAAGTGCTGGCTGATACCAAAGAACTGGTTAGCTCCAAAGTTTCT
GGCGCGCAGGAAATGGTTTCTTCCGCTAAAGACACCGTTGCTACCCAGCTGAGCGAAGCGGTAGACGCCACCCGTGGT
GCTGTTCAGTCTGGTGTTGATAAAACCAAATCCGTGGTTACCGGCGGTGTGCAGAGCGTTATGGGCAGCCGTCTGGGT
CAGATGGTTCTGAGCGGTGTTGACACCGTTCTGGGTAAATCTGAAGAATGGGCGGACAACCACCTTCCGCTGACCGAC
GCGGAACTGGCTCGCATCGCGACCTCTCTGGACGGTTTCGACGTTGCGAGCGTTCAGCAGCAGCGTCAGGAACAGTCT
TACTTCGTTCGTCTGGGTAGCCTGTCCGAACGTCTGCGTCAGCACGCTTACGAACACTCTCTGGGTAAACTGCGTGCT
ACCAAACAGCGTGCGCAGGAAGCTCTGCTGCAGCTGTCTCAGGTTCTGTCTCTGATGGAAACCGTTAAACAGGGTGTT
GACCAGAAACTGGTTGAAGGCCAGGAAAAACTGCACCAGATGTGGCTGTCTTGGAACCAGAAACAGCTGCAGGGTCCG
GAAAAAGAACCGCCGAAACCGGAACAGGTTGAATCCCGTGCTCTGACCATGTTCCGTGACATCGCGCAGCAGCTGCAG
GCTACCTGCACCTCCCTGGGTTCCTCTATCCAGGGTCTGCCGACCAACGTTAAAGACCAGGTTCAGCAGGCGCGTCGT
CAGGTTGAGGACCTGCAGGCGACCTTCAGCTCCATCCATTCTTTCCAGGACCTGTCCTCTTCTATCCTGGCTCAGTCC
CGTGAACGTGTAGCGTCTGCGCGTGAAGCGCTGGACCACATGGTTGAATACGTTGCTCAGAACACCCCGGTAACTTGG
CTGGTTGGTCCGTTCGCTCCGGGTATCACTGAAAAAGCTCCTGAAGAGAAAAAATAA
```